Structural Engineering and Mechanics, *Vol. 67, No. 2 (2018) 185-206*
DOI: https://doi.org/10.12989/sem.2018.67.2.185

Three-dimensional dynamics of the moving load acting on the interior of the hollow cylinder surrounded by the elastic medium

S. D. Akbarov*[1,2], M.A. Mehdiyev[3a] and M. Ozisik[4b]

[1]*Department of Mechanical Engineering, Faculty of Mechanical Engineering, Yildiz Technical University, Yildiz Campus, 34349 Besiktas, Istanbul, Turkey*
[2]*Institute of Mathematics and Mechanics, National Academy of Science of Azerbaijan, AZ1141, Baku, Azerbaijan*
[3]*Department of Mathematics, Azerbaijan State University of Economics (UNEC), 1001, Baku, Azerbaijan*
[4]*Department of Mathematical Engineering, Faculty of Chemistry and Metallurgy, Yildiz Technical University, Davutpasa Campus, 34220, Esenler, Istanbul, Turkey*

(Received April 20, 2018, Revised May 5, 2018, Accepted May 8, 2018)

Abstract. This paper studies the non-axisymmetric 3D problem on the dynamics of the moving load acting in the interior of the hollow cylinder surrounded with elastic medium and this study is made by utilizing the exact equations of elastodynamics. It is assumed that in the interior of the cylinder the point located with respect to the cylinder axis moving forces act and the distribution of these forces is non-axisymmetric and is located within a certain central angle. The solution to the problem is based on employing the moving coordinate method, on the Fourier transform with respect to the spatial coordinate indicated by the distance of the point on the cylinder axis from the point at which the moving load acts, and on the Fourier series presentation of the Fourier transforms of the sought values. Numerical results on the critical moving velocity and on the distribution of the interface normal and shear stresses are presented and discussed. In particular, it is established that the non-axisymmetricity of the moving load can decrease significantly the values of the critical velocity.

Keywords: non-axisymmetric moving load; critical velocity; hollow cylinder; elastic medium; interface stresses; Fourier series

1. Introduction

The study of the dynamic interface stress field in the bi-material elastic system consisting of the hollow cylinder and surrounding elastic or viscoelastic medium through which, as usual, underground structures are modelled and into which high-speed wheels move, has great significance not only in the theoretical sense, but also in the application sense. One of the main issues of systems subjected to the action of a moving load is to determine the velocity of this load, under a certain value of which, resonance type behavior of the system takes place and where the velocity which corresponds to this resonance is called the critical velocity. Another issue of the aforementioned system is to determine the stress-strain state on the interface surface between its constituents and the rules of attenuation of the perturbations of the stresses and displacements caused by the moving load with the distance from the point at which this load acts and with time. Investigations of these issues for the aforementioned bi-material system under action of a point located with respect to the cylinder's axis and which is non-axisymmetric in the circumferential direction of the distributed moving with constant velocity forces in the interior of the cylinder, are the subject of the present paper. For determination of the significance and place of the present investigations among others a brief review of corresponding investigations regarding layered elastic systems is considered below.

Apparently, the first attempt in this field was made in the paper by Achenbach, Keshava and Hermann (1967) in which the dynamics of the moving load acting on the "plate+half-space" system is investigated. The motion of the plate is described within the scope of the Timoshenko plate theory, however, the motion of the half-space is described by employing the exact equations of elastodynamics and the plane strain state is considered.

The investigations started in the paper by Achenbach, Keshava and Herman (1967) are developed in the papers by Dieterman and Metrikine (1997) and by Metrikine and Vrouwenvelder (2000) and others listed therein. Note that the paper by Dieterman and Metrikine (1997) studies the dynamics of the point-located time-harmonic varying moving load which acts on the infinite slab resting on a rigid foundation, and the 3D stress-strain state is considered. However, in the paper Metrikine and Vrouwenvelder (2000) it is assumed that the moving load acts on the beam which is embedded in the slab which also rests on the rigid foundation and the 2D stress-strain state is considered. The motion of the beam is written within the framework of the Euler-Bernoulli beam theory. Note that in

*Corresponding author, Professor
E-mail: akbarov@yildiz.edu.tr
[a]Professor
E-mail: mahirmehdiyev@mail.ru
[b]Ph.D.
E-mail: ozisik@yildiz.edu.tr

ISSN: 1225-4568 (Print), 1598-6217 (Online)

these works and other similar ones, the main attention is focused on determination of the critical velocity and on the displacement distribution caused by the moving load.

The dynamics of the moving load acting on the layered system is also studied in the papers by Akbarov *et al*. (2007), Akbarov and Ilhan (2008), Akbarov and Ilhan (2009), Dincsoy *et al*. (2009), Babich *et al.* (1986), Babich *et al*. (1988), Babich *et al*. 2008a, b, Akbarov and Salmanova (2009), Akbarov *et al*. (2015) and others listed therein, which are also discussed in the monograph by Akbarov (2015). Note that in these papers it is assumed that the existence of initial stresses in the layers and their motion are described by utilizing the so-called three-dimensional linearized equations of wave propagation in initially stressed elastic bodies. Moreover, note that in these works, not only the critical velocities of the moving load, but also the interface stresses caused by this moving load have been investigated.

The dynamic response on the moving load acting on a Bernoulli-Euler beam supported with poroelasticity subgrade material is investigated in the paper by Shi and Selvadurai (2016) by employing the concept of the equivalent stiffness of the half-space.

The 3D steady-state dynamic response of the multi-layered transversely isotropic half-space generated by a point-located moving load with constant velocity acting on the face plane of this half-space is investigated in the paper by Zhenning *et al*. (2016), in which it is assumed that the packet of layers made of hysteretic viscoelastic transversely isotropic materials lies on a half-space which is also made from a hysteretic viscoelastic transversely isotropic material.

This completes the review of the investigations related to the plane-layered systems. Here, we do not consider a review of the investigations related to the action of the moving load on beams, plates and other types of elements of construction. However, we note that the corresponding review is made in the paper by Quyang (2011). At the same time, we note that the more recent investigations in this field are made in the papers by Sarvestan *et al.* (2017), Song *et al*. (2016), Sudheesh *et al.* (2015), Kiani *et al*. (2015) and in other ones listed therein.

Thus, after the foregoing discussions we consider a review of the investigations related to the dynamics of the moving load acting in the interior of the cylindrical bore (cavity) with infinite length within the infinite homogeneous and cylindrically layered medium. This review can begin with the paper by Parnes (1969) in which the dynamics of a line load applied along a transverse circle moving with constant velocity in the axial direction along the interior of a circular bore in an infinite homogeneous elastic medium, are investigated. It is assumed that the velocity of the moving load is greater than the shear wave's velocities in the elastic medium, i.e., the supersonic regime is considered and although the theoretical analyses are made for the 3D problem, the numerical results on the stress and displacements are presented only for the axisymmetric case, i.e., for the corresponding 2D problem.

The paper by Parnes (1980) studies the problem considered in the previous paper by this author for the case where in the interior of the cylindrical cavity a torsional moving load acts. Note that in the papers by Parnes (1969), Parnes (1980) the question related to the critical velocity is not considered. Rather, the question on the determination of the critical velocity of the moving load acting on infinite (as in the papers by Parnes (1969), Parnes (1980) or semi-infinite mediums does not appear in the cases where these mediums are homogeneous. Thus, the question related to the determination of the critical velocity relates only to the moving load acting on the piece-wise inhomogeneous bodies including the piece-wise inhomogeneous infinite (for instance, for the system consisting of a hollow cylinder surrounded with elastic medium) or semi-infinite (for instance, for the system consisting of a covering layer and half-space) bodies. What is more, the critical velocity in these infinite and semi-infinite bodies appears only in the cases where the modulus of elasticity of the covering layer material is greater than that of the surrounding infinite medium or of the stratified semi-infinite medium. In connection with this, it is necessary to take into consideration these discussions under investigations of the problem related to the dynamics of the moving load acting on the piece-wise inhomogeneous infinite cylindrically layered systems which are considered in the papers by Chonan (1981), Pozhuev (1980), Abdulkadirov (1981), Hasheminejad and Komeili (2009) and others listed therein.

The dynamic response of a cylindrical shell imperfectly bonded to a surrounding infinite elastic continuum under action of axisymmetric ring pressure which moves with constant velocity in the axial direction along the interior of the shell is studied in the paper by Chonan (1981). The motion of the shell is described by thick shell theories and the motion of the surrounding elastic medium is described by the exact equations of linear elastodynamics. It is assumed that the shell and the surrounding elastic medium are joined together by a thin elastic bond. Numerical results on the critical speed of the moving load and on the radial displacement of the shell for the subcritical moving load are presented and discussed.

The paper by Pozhuev (1980) studies the moving load problem for the system consisting of a thin cylindrical shell and surrounding transversally isotropic infinite medium. A thin shell theory is employed for describing the motion of the cylindrical shell, however, the motion of the continuum is described with the exact equations of motion of elastodynamics for transversally isotropic bodies. In this paper a few numerical results regarding displacements and a radial normal stress are presented, but there are no numerical results related to the critical velocity of the moving load.

The critical velocity of the moving ring load acting on the system "hollow cylinder+surrounding elastic medium" is also studied in the paper by Abdulkadirov (1981). However, this study is made through the investigation of low-frequency resonance axisymmetric longitudinal waves propagated in this system and under "resonance waves", the cases for which the relation dc/dk=0 occurs, are understood, where c is the wave propagation velocity and k is the wavenumber. The velocity of these "resonance waves" is taken as the critical velocity of the corresponding moving

load. Investigations are made by utilizing the exact equations of elastodynamics in the axisymmetric case and some numerical examples of "resonance waves" are presented and discussed.

The paper by Hasheminejad and Komeili (2009) studies the effect of imperfect bonding on the axisymmetric elastodynamic response of the system consisting of an isotropic hollow cylinder and surrounding poroelastic soil due to a moving ring load. Numerical examples on the critical velocity of the moving load are also considered.

The paper by Zhou *et al*. (2008) studies the critical velocity of the moving internal pressure acting in the cylindrical layered system with finite thickness. Two types of approaches are used, the first of which is based on first order refined sandwich shell theories, while the second approach is based on the exact equations of linear elastodynamics for orthotropic bodies with effective mechanical constants. Numerical results on the critical velocity obtained within these approaches are compared, from which it follows that, as can be predicted, they are sufficiently close to each other for the low wavenumber cases, however, the difference between these results increases with the wavenumber and becomes so great that it appears necessary to determine which approach is more accurate. However, for this determination it is necessary to investigate these problems by employing the exact field equations of elastodynamics within the scope of the piecewise homogeneous body model, which is also used in the paper by Akbarov and Mehdiyev (2017) under investigation of the axisymmetric time-harmonic forced vibration of the "hollow cylinder+surrounding elastic medium" system. Note that the approach based on the exact equations of elastodynamics within the scope of the piece-wise homogeneous body model is also employed in the present paper.

Recently in the paper by Ozisik *et al*. (2018) the problem related to the dynamics of the axisymmetric moving ring load acting on the interior of the cylinder surrounded with the elastic medium has been studied. This study is also made within the scope of the exact equations and relations of the elastodynamics and the main attention is focused on the influence of the imperfectness of the contact conditions between the constituents of the system on the critical velocity of the moving load. Moreover, in the paper by Akbarov and Mehdiyev (2018a) it is studied the influence of the homogeneous initial stresses appearing as a result of the uniaxial stretching or compression of the system "hollow cylinder+surrounding elastic medium" on the critical velocity of the moving ring load and on the interface stress state in this system.

Note that the all foregoing investigations carried out within the scope of the exact equations and relations of the elastodynamics relate to the axisymmetric stress state case. In the paper Akbarov and Mehdiyev (2018b) it is made the first attempt to study the 3D non-axisymmetric problem for the system "hollow cylinder+surrounding elastic medium" under action the time-harmonic forces distributed in a certain part of the interior of the cylinder. As a result of this study, it is established that the non-axisymmetricity of the external time-harmonic force cause to increase of the absolute values of the interface stresses in the system under consideration with respect to those obtained in the corresponding axisymmetric case. It should be also indicated that the corresponding dynamic problems for the hydro-elastic system are investigated in the papers by Akbarov and Ismailov (2014), Akbarov and Ismailov (2015), Akbarov and Ismailov (2016a), Akbarov and Ismailov (2016b), Akbarov and Ismailov (2017), Akbarov and Panakhli (2015), Akbarov and Panakhli (2017) and others listed therein.

Finally, we note the papers Forrest and Hunt (2006), Sheng, Jones and Thompson (2006), Hung *et al.* (2013), Hussein *et al*. (2014), Yuan *et al*. (2017) and others listed therein, in which numerical and analytical solution methods have been developed for studying the dynamical response of tunnel (modelled as a hollow elastic cylinder)+soil (modelled as surrounding elastic or viscoelastic medium) systems generated by the moving load acting on the interior of the tunnels. However, the focus in these investigations is on the displacement distribution of the soils caused by the moving load and the analyses related to the critical velocity and to the response of the interface stresses to the moving load are almost completely absent.

It should be noted that the results of the study of the aforementioned response of the interface stresses to the moving load and of the study of the critical velocity of this load have great significance for estimation of the adhesion strength of the "hollow cylinder+surrounding elastic medium" system.

The other aspect of related investigations is the modelling of the external moving load which as usual is modelled as an axisymmetric ring load. However, this model is not more realistic in many practical cases and so the non-axisymmetric loading model of the moving load is more suitable even though this model complicates significantly the solution procedure of the corresponding boundary-value problems. This is because in the non-axisymmetric moving load case it is necessary to solve the corresponding 3D problem in the cylindrical coordinate system. However, despite the complications of the solution procedure, the model based on the non-axisymmetric moving load case allows us to answer the following:

- whether the values of the critical speed of the moving load depend on the non-axisymmetricity of this load or whether the critical velocity determined for the corresponding axisymmetric moving load case occurs also for the non-axisymmetric moving load case;
- what area of the interior surface of the hollow cylinder is more suitable in the sense of the maximum interface stresses for distribution of the moving load with a constant vertical (normal) component;
- how the interface stress distributions depend on the non-axisymmetricity of the moving load and how the problem parameters act on these distributions etc.

Namely, the study of the foregoing issues is the subject of the present paper.

2. Formulation of the problem and governing field equations

Consider a system consisting of a hollow circular

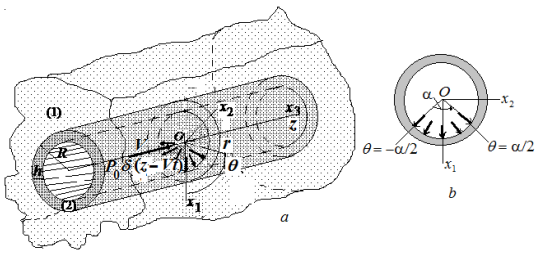

Fig. 1(a) The sketch of the considered system and (b) the sketch of the distribution of the non-axisymmetric normal forces

cylinder with thickness h and with external radius R and of an infinite surrounding elastic medium, a sketch of which is shown in Fig. 1 and associate the cylindrical system of coordinates $Orz\theta$ with the axis of the cylinder. Assume that in the interior of the cylinder there is a point located with respect to the cylinder axis and that non-uniformly distributed in the circumferential direction moving normal forces act and these forces move with constant velocity V in the Oz axis direction Fig. 1. In the present paper, within this framework we attempt to investigate the non-axisymmetric dynamic response of the system to these moving forces.

Below, the values related to the cylinder will be denoted by the upper index (2), however, the values related to the surrounding elastic medium will be denoted by the upper index (1).

We assume that the materials of the constituents are homogeneous and isotropic. Now we write the corresponding 3D field equations and boundary and contact conditions.

Equations of motion

$$\frac{\partial \sigma_{rr}^{(m)}}{\partial r}+\frac{1}{r}\frac{\partial \sigma_{r\theta}^{(m)}}{\partial \theta}+\frac{\partial \sigma_{rz}^{(m)}}{\partial z}+\frac{1}{r}(\sigma_{rr}^{(m)}-\sigma_{\theta\theta}^{(m)})=\rho^{(m)}\frac{\partial^2 u_r^{(m)}}{\partial t^2}$$

$$\frac{\partial \sigma_{r\theta}^{(m)}}{\partial r}+\frac{1}{r}\frac{\partial \sigma_{\theta\theta}^{(m)}}{\partial \theta}+\frac{\partial \sigma_{z\theta}^{(m)}}{\partial z}+\frac{2}{r}\sigma_{r\theta}^{(m)}=\rho^{(m)}\frac{\partial^2 u_\theta^{(m)}}{\partial t^2} \qquad (1)$$

$$\frac{\partial \sigma_{rz}^{(m)}}{\partial r}+\frac{1}{r}\frac{\partial \sigma_{z\theta}^{(m)}}{\partial \theta}+\frac{\partial \sigma_{zz}^{(m)}}{\partial z}+\frac{1}{r}\sigma_{rz}^{(m)}=\rho^{(m)}\frac{\partial^2 u_z^{(m)}}{\partial t^2}$$

Elasticity relations

$$\sigma_{rr}^{(m)}=(\lambda^{(m)}+2\mu^{(m)})\frac{\partial u_r^{(m)}}{\partial r}+\lambda^{(m)}\frac{1}{r}(\frac{\partial u_\theta^{(m)}}{\partial r}+u_r^{(m)})+\lambda^{(m)}\frac{\partial u_z^{(m)}}{\partial z}$$

$$\sigma_{\theta\theta}^{(m)}=\lambda^{(m)}\frac{\partial u_r^{(m)}}{\partial r}+(\lambda^{(m)}+2\mu^{(m)})\frac{1}{r}(\frac{\partial u_\theta^{(m)}}{\partial r}+u_r^{(m)})+\lambda^{(m)}\frac{\partial u_z^{(m)}}{\partial z}$$

$$\sigma_{zz}^{(m)}=\lambda^{(m)}\frac{\partial u_r^{(m)}}{\partial r}+\lambda^{(m)}\frac{1}{r}(\frac{\partial u_\theta^{(m)}}{\partial r}+u_r^{(m)})+(\lambda^{(m)}+2\mu^{(m)})\frac{\partial u_z^{(m)}}{\partial z} \qquad (2)$$

$$\sigma_{r\theta}^{(m)}=\mu^{(m)}\frac{\partial u_\theta^{(m)}}{\partial r}+\mu^{(m)}(\frac{1}{r}\frac{\partial u_r^{(m)}}{\partial \theta}-\frac{1}{r}u_\theta^{(m)})$$

$$\sigma_{z\theta}^{(m)}=\mu^{(m)}\frac{\partial u_\theta^{(m)}}{\partial z}+\mu^{(k)}\frac{\partial u_z^{(m)}}{r\partial \theta},$$

$$\sigma_{zr}^{(k)}=\mu^{(k)}\frac{\partial u_r^{(k)}}{\partial z}+\mu^{(k)}\frac{\partial u_z^{(k)}}{\partial r}$$

In Eqs. (1)-(2) a conventional notation is used.

According to the foregoing discussions and to Fig. 1(b), the following boundary conditions can be written.

$$\sigma_{rr}^{(2)}\Big|_{r=R-h}=\begin{cases}-P_\alpha\delta(z-Vt) & \text{for } -\alpha/2\le\theta\le\alpha/2\\ 0 & \text{for } \theta\in\left([-\pi,+\pi]-[-\alpha/2,\alpha/2]\right)\end{cases} \qquad (3)$$

$$\sigma_{r\theta}^{(2)}\Big|_{r=R-h}=0\,,\quad \sigma_{rz}^{(2)}\Big|_{r=R-h}=0$$

where P_α is determined from the following relation.

$$\int_{-\alpha/2}^{+\alpha/2}P_\alpha(R-h)\cos\theta\,\mathrm{d}\theta=(R-h)P_0=const \qquad (4)$$

$$\Rightarrow P_\alpha=P_0/(2\sin(\alpha/2))$$

i.e., the vertical component of the summation of the external forces does not depend on the angle α Fig. 1(b) and this summation is constant.

We assume that perfect contact conditions are satisfied, i.e., it is assumed that

$$\sigma_{rr}^{(2)}\Big|_{r=R}=\sigma_{rr}^{(1)}\Big|_{r=R},\ \sigma_{r\theta}^{(2)}\Big|_{r=R}=\sigma_{r\theta}^{(1)}\Big|_{r=R}$$
$$\sigma_{rz}^{(2)}\Big|_{r=R}=\sigma_{rz}^{(1)}\Big|_{r=R},\ u_r^{(2)}\Big|_{r=R}=u_r^{(1)}\Big|_{r=R} \qquad (5)$$
$$u_\theta^{(2)}\Big|_{r=R}=u_\theta^{(1)}\Big|_{r=R},\ u_z^{(2)}\Big|_{r=R}=u_z^{(1)}\Big|_{r=R}$$

Moreover, we assume that

$$V<\min\left\{c_2^{(2)};c_2^{(1)}\right\}$$
$$c_2^{(m)}=\sqrt{\mu^{(m)}/\rho^{(m)}}\,,\quad m=1,2 \qquad (6)$$

i.e., the subsonic regime is considered. According to assumption Eq. (6), it can be concluded that the following decay conditions must be satisfied

$$\left\{\sigma_{rr}^{(2)};\sigma_{r\theta}^{(2)};...;\sigma_{z\theta}^{(2)};u_r^{(2)};...;u_z^{(2)}\right\}\to 0$$
$$\text{as}\quad |z-Vt|\to+\infty$$
$$\left\{\sigma_{rr}^{(1)};\sigma_{r\theta}^{(1)};...;\sigma_{z\theta}^{(1)};u_r^{(1)};...;u_z^{(1)}\right\}\to 0 \qquad (7)$$
$$\text{as}\quad \sqrt{r^2+(z-Vt)^2}\to+\infty$$

This completes the formulation of the problem.

3. Method of solution

For solution of the boundary value problem Eqs. (1)-(7), according to Guz (1999), we use the following representation

$$u_r^{(m)}=\frac{1}{r}\frac{\partial}{\partial\theta}\Psi^{(m)}-\frac{\partial^2}{\partial r\partial z}X^{(m)}$$
$$u_\theta^{(m)}=-\frac{\partial}{\partial r}\Psi^{(m)}-\frac{1}{r}\frac{\partial^2}{\partial\theta\partial z}X^{(m)} \qquad (8)$$

$$u_z^{(m)} = (\lambda^{(m)} + \mu^{(m)})^{-1}\left((\lambda^{(m)} + 2\mu^{(m)})\Delta_1 + \mu^{(m)}\frac{\partial^2}{\partial z^2} - \rho^{(m)}\frac{\partial^2}{\partial t^2}\right)X^{(m)}$$

$$\Delta_1 = \frac{\partial^2}{\partial r^2} + \frac{1}{r}\frac{\partial}{\partial r} + \frac{1}{r^2}\frac{\partial^2}{\partial \theta^2}, \quad m = 1,2$$

Here the functions $\Psi^{(m)}$ and $X^{(m)}$ are the solutions of the equations

$$\left(\Delta_1 + \frac{\partial^2}{\partial z^2} - \frac{\rho^{(k)}}{\mu^{(k)}}\frac{\partial^2}{\partial t^2}\right)\Psi^{(m)} = 0$$

$$\left[\left(\Delta_1 + \frac{\partial^2}{\partial z^2}\right)\left(\Delta_1 + \frac{\partial^2}{\partial z^2}\right) + -\rho^{(m)}\frac{\lambda^{(m)} + 3\mu^{(m)}}{\mu^{(m)}(\lambda^{(m)} + 2\mu^{(m)})}\right. \tag{9}$$

$$\left.(\Delta_1 + \frac{\partial^2}{\partial z^2})\right)\frac{\partial^2}{\partial t^2} + \frac{(\rho^{(m)})^2}{\mu^{(m)}(\lambda^{(m)} + 2\mu^{(m)})}\frac{\partial^4}{\partial t^4}\Bigg]X^{(m)} = 0$$

We introduce a moving cylindrical coordinate system *O'r'z'θ'* which is connected with the reference cylindrical coordinate system *Orzθ* through the following relations

$$r' = r, \quad \theta' = \theta, \quad z' = z - Vt \tag{10}$$

Replacing the operators $\partial^2/\partial t^2$ and $\partial^4/\partial t^4$ with the operators $V^2/\partial^2/\partial z'^2$ and $V^4/\partial^4/\partial z'^4$, respectively, the foregoing equations and relations rewritten in the moving coordinate system, are obtained. Further, the exponential Fourier transform $f_F = \int_{-\infty}^{+\infty} f(z')e^{isz'}dz'$ with respect to the moving coordinate *z'* (where *s* is a transformation parameter) is applied to all the equations and relations rewritten with the moving coordinates.

Below, all mathematical operations will be made with the use of the moving coordinates and their upper primes will be omitted.

Thus, according to the symmetry and asymmetry of the sought values with respect to the plane *z*=0, their originals can be presented through their Fourier transforms by the following relations.

$$\left\{\sigma_{rr}^{(m)};\sigma_{\theta\theta}^{(m)};\sigma_{zz}^{(m)};\sigma_{r\theta}^{(m)};u_r^{(m)};u_\theta^{(m)};\Psi^{(m)}\right\} = \frac{1}{\pi}\int_0^{+\infty}\left\{\sigma_{rrF}^{(m)};\sigma_{\theta\theta F}^{(m)};\sigma_{zzF}^{(m)};\sigma_{r\theta F}^{(m)};u_{rF}^{(m)};u_{\theta F}^{(m)};\Psi_F^{(m)}\right\}\cos(sz)ds$$

$$\left\{\sigma_{\theta z}^{(m)};\sigma_{rz}^{(m)};u_z^{(m)};X^{(m)}\right\} = \frac{1}{\pi}\int_0^{+\infty}\left\{\sigma_{\theta zF}^{(m)};\sigma_{rzF}^{(m)};u_{zF}^{(m)};X_F^{(m)}\right\}\sin(sz)ds \tag{11}$$

Substituting the expressions in Eq. (11) into the foregoing equations and the rewritten relations in the moving coordinate system, it is obtained the following equations for the functions $\Psi_F^{(m)}$ and $X_F^{(m)}$

$$\left(\Delta_1 - s^2(1 - \frac{\rho^{(k)}}{\mu^{(k)}}V^2)\right)\Psi_F^{(m)} = 0$$

$$\left[\left(\Delta_1 - s^2\right)\left(\Delta_1 - s^2\right) + -\rho^{(m)}\frac{\lambda^{(m)} + 3\mu^{(m)}}{\mu^{(m)}(\lambda^{(m)} + 2\mu^{(m)})}\right. \tag{12}$$

$$\left.(\Delta_1 - s^2)\right)(-s^2V^2) + \frac{(\rho^{(m)})^2}{\mu^{(m)}(\lambda^{(m)} + 2\mu^{(m)})}s^4V^4\Bigg]X_F^{(m)} = 0$$

According to the nature of the problem under consideration, the Fourier transform of the functions $\Psi_F^{(m)}$ and $X_F^{(m)}$ can be presented in the Fourier series form as follows.

$$\Psi_F^{(m)}(r,s,\theta) = \sum_{n=1}^{\infty}\Psi_{Fn}^{(m)}(r,s)\sin n\theta$$

$$X_F^{(m)}(r,s,\theta) = \frac{1}{2}X_{F0}^{(m)}(r,s) + \sum_{n=1}^{\infty}X_{Fn}^{(m)}(r,s)\cos n\theta \tag{13}$$

Substituting expressions Eq. (13) into the equations in Eq. (12), the equations given below are obtained for the unknown functions $\Psi_{Fn}^{(m)}(r,s)$ and $X_{Fn}^{(m)}(r,s)$.

$$\left(\Delta_{1n} - (\zeta_1^{(m)})^2\right)\psi_{Fn}^{(m)} = 0$$

$$\left(\Delta_{1n} - (\zeta_2^{(m)})^2\right)\left(\Delta_{1n} - (\zeta_3^{(m)})^2\right)X_{Fn}^{(m)} = 0 \tag{14}$$

$$\Delta_{1n} = \frac{\mathrm{d}^2}{\mathrm{d}r^2} + \frac{\mathrm{d}}{r\mathrm{d}r} - \frac{n^2}{r^2}$$

where

$$(\zeta_1^{(m)})^2 = s^2\left(1 - \frac{\rho^{(m)}V^2}{\mu^{(m)}}\right) \tag{15}$$

$(\zeta_2^{(m)})^2$ and $(\zeta_2^{(m)})^2$ in Eq. (14) are determined as solutions of the following equation.

$$\mu^{(m)}(\zeta^{(m)})^4 - s^2(\zeta^{(m)})^2\left[-\rho^{(m)}V^2 - (\lambda^{(m)} + 2\mu^{(m)})\right.$$

$$\left. + \frac{\mu^{(m)}}{\lambda^{(m)} + 2\mu^{(m)}}\left(-\rho^{(m)}V^2 - \mu^{(m)}\right) + \frac{(\lambda^{(m)} + \mu^{(m)})^2}{\lambda^{(m)} + 2\mu^{(m)}}\right] + \tag{16}$$

$$s^4\left(\frac{-\rho^{(m)}V^2}{\lambda^{(m)} + 2\mu^{(m)}} - 1\right)\left(-\rho^{(m)}V^2 - \mu^{(m)}\right) = 0$$

Thus, according to the conditions Eqs. (6)-(7), the solution to the equations in Eq. (14) is found as follows.

For the hollow cylinder

$$\psi_{Fn}^{(2)} = A_{1n}^{(2)}I_n(\zeta_1^{(2)}r) + B_{1n}^{(2)}K_n(\zeta_1^{(2)}r)$$

$$\chi_{Fn}^{(2)} = A_{2n}^{(2)}I_n(\zeta_2^{(2)}r) + A_{3n}^{(2)}I_n(\zeta_3^{(2)}r) + \tag{17}$$

$$B_{2n}^{(2)}K_n(\zeta_2^{(2)}r) + B_{3n}^{(2)}K_n(\zeta_3^{(2)}r)$$

For the surrounding elastic medium

$$\psi_{Fn}^{(1)} = B_{1n}^{(1)} K_n(\zeta_1^{(1)} r)$$
$$\chi_{Fn}^{(1)} = B_{2n}^{(1)} K_n(\zeta_2^{(1)} r) + B_{3n}^{(1)} K_n(\zeta_3^{(1)} r) \quad (18)$$

In Eqs. (17)-(18), $I_n(x)$ and $K_n(x)$ are the modified Bessel functions of the $n-th$ order of the first and second kinds, respectively. Moreover, in Eqs. (17)-(18), $B_{1n}^{(1)}$, $B_{2n}^{(1)}$, $B_{3n}^{(1)}$, $A_{1n}^{(2)}$, $A_{2n}^{(2)}$, $A_{3n}^{(2)}$, $B_{1n}^{(2)}$, $B_{2n}^{(2)}$ and $B_{3n}^{(2)}$ are unknown constants which will be determined from the boundary Eq. (3) and contact Eq. (5) conditions.

Thus, substituting expressions Eqs. (17)-(18) and Eq. (13) into the equations in Eq. (8) and Eq. (2), we obtain the following expressions for the stresses and displacements which enter into the boundary and contact conditions given in Eq. (3) and Eq. (5).

For the surrounding elastic medium

$$\frac{\sigma_{rrF}^{(1)}(r,s)}{\mu^{(1)}} = B_{20}^{(1)} b_{120}(r) + B_{30}^{(1)} b_{130}(r) + \sum_{n=1}^{\infty}\left[B_{1n}^{(1)} b_{11n}(r) + B_{2n}^{(1)} b_{12n}(r) + B_{3n}^{(1)} b_{13n}(r)\right]\cos(n\theta)$$

$$\frac{\sigma_{r\theta F}^{(1)}(r,s)}{\mu^{(1)}} = \sum_{n=1}^{\infty}\left[B_{1n}^{(1)} b_{21n}(r) + B_{2n}^{(1)} b_{22n}(r) + B_{3n}^{(1)} b_{23n}(r)\right]\sin(n\theta)$$

$$\frac{\sigma_{rzF}^{(1)}(r,s)}{\mu^{(1)}} = B_{20}^{(1)} b_{320}(r) + B_{30}^{(1)} b_{330}(r) + \sum_{n=1}^{\infty}\left[B_{1n}^{(1)} b_{31n}(r) + B_{2n}^{(1)} b_{32n}(r) + B_{3n}^{(1)} b_{33n}(r)\right]\cos(n\theta)$$

$$u_{rF}^{(1)}(r,s) = B_{20}^{(1)} b_{420}(r) + B_{30}^{(1)} b_{430}(r) + \sum_{n=1}^{\infty}\left[B_{1n}^{(1)} b_{41n}(r) + B_{2n}^{(1)} b_{42n}(r) + B_{3n}^{(1)} b_{43n}(r)\right]\cos(n\theta)$$

$$u_{\theta F}^{(1)}(r,s) = \sum_{n=1}^{\infty}\left[B_{1n}^{(1)} b_{51n}(r) + B_{2n}^{(1)} b_{52n}(r) + B_{3n}^{(1)} b_{53n}(r)\right]\sin(n\theta)$$

$$u_{zF}^{(1)}(r,s) = B_{20}^{(1)} b_{620}(r) + B_{30}^{(1)} b_{630}(r) + \sum_{n=1}^{\infty}\left[B_{1n}^{(1)} b_{61n}(r) + B_{2n}^{(1)} b_{62n}(r) + B_{3n}^{(1)} b_{63n}(r)\right]\cos(n\theta) \quad (19)$$

For the hollow cylinder

$$\frac{\sigma_{rrF}^{(2)}(r,s)}{\mu^{(2)}} = A_{20}^{(2)} d_{120}(r) + A_{30}^{(2)} d_{130}(r) + B_{20}^{(2)} c_{120}(r) + B_{30}^{(2)} c_{130}(r) + \sum_{n=1}^{\infty}\left[A_{1n}^{(2)} d_{11n}(r) + A_{2n}^{(2)} d_{12n}(r) + A_{3n}^{(2)} d_{13n}(r) + B_{1n}^{(2)} c_{11n}(r) + B_{2n}^{(2)} c_{12n}(r) + B_{3n}^{(2)} c_{13n}(r)\right]\cos(n\theta) \quad (15)$$

$$\frac{\sigma_{r\theta F}^{(2)}(r,s)}{\mu^{(2)}} = \sum_{n=1}^{\infty}\left[A_{1n}^{(2)} d_{21n}(r) + A_{2n}^{(2)} d_{22n}(r) + A_{3n}^{(2)} d_{23n}(r) + B_{1n}^{(2)} c_{21n}(r) + B_{2n}^{(2)} c_{22n}(r) + B_{3n}^{(2)} c_{23n}(r)\right]\cos(n\theta)$$

$$\frac{\sigma_{rzF}^{(2)}(r,s)}{\mu^{(2)}} = A_{20}^{(2)} d_{320}(r) + A_{30}^{(2)} d_{330}(r) + B_{20}^{(2)} c_{320}(r) + B_{30}^{(2)} c_{330}(r) + \sum_{n=1}^{\infty}\left[A_{1n}^{(2)} d_{31n}(r) + A_{2n}^{(2)} d_{32n}(r) + A_{3n}^{(2)} d_{33n}(r) + B_{1n}^{(2)} c_{31n}(r) + B_{2n}^{(2)} c_{32n}(r) + B_{3n}^{(2)} c_{33n}(r)\right]\cos(n\theta)$$

$$u_{rF}^{(2)}(r,s) = A_{20}^{(2)} d_{420}(r) + A_{30}^{(2)} d_{430}(r) + B_{20}^{(2)} c_{420}(r) + B_{30}^{(2)} c_{430}(r) + \sum_{n=1}^{\infty}\left[A_{1n}^{(2)} d_{41n}(r) + A_{2n}^{(2)} d_{42n}(r) + A_{3n}^{(2)} d_{43n}(r) + B_{1n}^{(2)} c_{41n}(r) + B_{2n}^{(2)} c_{42n}(r) + B_{3n}^{(2)} c_{43n}(r)\right]\cos(n\theta)$$

$$u_{\theta F}^{(2)}(r,s) = \sum_{n=1}^{\infty}\left[A_{1n}^{(2)} d_{51n}(r) + A_{2n}^{(2)} d_{52n}(r) + A_{3n}^{(2)} d_{53n}(r) + B_{1n}^{(2)} c_{51n}(r) + B_{2n}^{(2)} c_{52n}(r) + B_{3n}^{(2)} c_{53n}(r)\right]\cos(n\theta)$$

$$u_{zF}^{(2)}(r,s) = A_{20}^{(2)} d_{620}(r) + A_{30}^{(2)} d_{630}(r) + B_{20}^{(2)} c_{620}(r) + B_{30}^{(2)} c_{630}(r) + \sum_{n=1}^{\infty}\left[A_{1n}^{(2)} d_{61n}(r) + A_{2n}^{(2)} d_{62n}(r) + A_{3n}^{(2)} d_{63n}(r) + B_{1n}^{(2)} c_{61n}(r) + B_{2n}^{(2)} c_{62n}(r) + B_{3n}^{(2)} c_{63n}(r)\right]\cos(n\theta)$$

The explicit expressions of the functions $b_{k1n}(r)$, $b_{k2n}(r)$, $b_{k3n}(r)$, $d_{k1n}(r)$, $d_{k2n}(r)$, $d_{k3n}(r)$, $c_{k1n}(r)$, $c_{k2n}(r)$ and $c_{k3n}(r)$ which enter into equations Eqs. (19)-(20) are given in Appendix A through the formulas (A1) and (A2).

Analysis of the Fourier transformation of the boundary Eq. (3) and contact Eq. (5) conditions shows that the second and third conditions in Eq. (3), and all the contact conditions in Eq. (5) remain valid as for the corresponding Fourier transforms. However, the first condition in Eq. (3) is transformed to the following one.

$$\sigma_{rrF}^{(2)}\Big|_{r=R-h} = \begin{cases} -P_\alpha & \text{for } -\alpha/2 \le \theta \le \alpha/2 \\ 0 & \text{for } \theta \in \left([-\pi,+\pi]-[-\alpha/2,\alpha/2]\right) \end{cases} \quad (21)$$

According to the well-known expansion procedure for the Fourier transform, the condition Eq. (21) can be presented in a series form as given below.

$$\sigma_{rrF}^{(2)}\Big|_{r=R-h}=-\frac{\alpha}{2\pi}P_\alpha-\frac{2\sin(\alpha/2)}{\pi}P_\alpha\sum_{n=1}^{\infty}\frac{1}{n}\cos(n\theta) \tag{22}$$

Thus, using the expressions in Eq. (20), we obtain the following equations for the unknown constants $A_{20}^{(2)}$, $A_{30}^{(2)}$, $B_{20}^{(2)}$, $B_{30}^{(2)}$, $B_{20}^{(1)}$, $B_{30}^{(1)}$, $B_{1n}^{(1)}$, $B_{2n}^{(1)}$, $B_{3n}^{(1)}$ $A_{1n}^{(2)}$, $A_{2n}^{(2)}$, $A_{3n}^{(2)}$, $B_{1n}^{(2)}$, $B_{2n}^{(2)}$ and $B_{3n}^{(2)}$ ($n\geq 1$) from the boundary condition Eq. (22), the second and third boundary conditions in Eq. (3) and from the contact conditions in Eq. (5).

For the unknown constants $A_{20}^{(2)}$, $A_{30}^{(2)}$, $B_{20}^{(2)}$, $B_{30}^{(2)}$, $B_{20}^{(1)}$ and $B_{30}^{(1)}$

$$\begin{gathered}
\mu^{(2)}\left(A_{20}^{(2)}d_{120}(r)+A_{30}^{(2)}d_{130}(r)+B_{20}^{(2)}c_{120}(r)\right.\\
\left.+B_{30}^{(2)}c_{130}(r)\right)_{r=R-h}=-\frac{\alpha}{2\pi}P_\alpha\\
\mu^{(2)}\left(A_{20}^{(2)}d_{320}(r)+A_{30}^{(2)}d_{330}(r)+B_{20}^{(2)}c_{320}(r)+\right.\\
\left.B_{30}^{(2)}c_{330}(r)\right)_{r=R-h}=0\\
\mu^{(2)}\left(A_{20}^{(2)}d_{120}(r)+A_{30}^{(2)}d_{130}(r)+B_{20}^{(2)}c_{120}(r)+\right.\\
\left.+B_{30}^{(2)}c_{130}(r)\right)_{r=R}=\mu^{(1)}\left(B_{20}^{(1)}b_{120}(r)+B_{30}^{(1)}b_{130}(r)\right)_{r=R}\\
\mu^{(2)}\left(A_{20}^{(2)}d_{320}(r)+A_{30}^{(2)}d_{330}(r)+B_{20}^{(2)}c_{320}(r)+\right.\\
\left.B_{30}^{(2)}c_{330}(r)\right)_{r=R}=\mu^{(1)}\left(B_{20}^{(1)}b_{320}(r)+B_{30}^{(1)}b_{330}(r)\right)_{r=R}\\
\left(A_{20}^{(2)}d_{420}(r)+A_{30}^{(2)}d_{430}(r)+B_{20}^{(2)}c_{420}(r)+\right.\\
\left.B_{30}^{(2)}c_{430}(r)\right)_{r=R}=\left(B_{20}^{(1)}b_{420}(r)+B_{30}^{(1)}b_{430}(r)\right)_{r=R}\\
\left(A_{20}^{(2)}d_{620}(r)+A_{30}^{(2)}d_{630}(r)+B_{20}^{(2)}c_{620}(r)+\right.\\
\left.B_{30}^{(2)}c_{630}(r)\right)_{r=R}=\left(B_{20}^{(1)}b_{620}(r)+B_{30}^{(1)}b_{630}(r)\right)_{r=R}
\end{gathered} \tag{23}$$

For the unknown constants $B_{1n}^{(1)}$, $B_{2n}^{(1)}$, $B_{3n}^{(1)}$ $A_{1n}^{(2)}$, $A_{2n}^{(2)}$, $A_{3n}^{(2)}$, $B_{1n}^{(2)}$, $B_{2n}^{(2)}$ and $B_{3n}^{(2)}$ ($n\geq 1$)

$$\begin{gathered}
\mu^{(2)}\left(A_{1n}^{(2)}d_{11n}(r)+A_{2n}^{(2)}d_{12n}(r)+A_{3n}^{(2)}d_{13n}(r)+\right.\\
\left.B_{1n}^{(2)}c_{11n}(r)+B_{2n}^{(2)}c_{12n}(r)+B_{3n}^{(2)}c_{13n}(r)\right)_{r=R-h}\\
=-\frac{2\sin(\alpha/2)}{\pi n}P_\alpha\\
\mu^{(2)}\left(A_{1n}^{(2)}d_{21n}(r)+A_{2n}^{(2)}d_{22n}(r)+A_{3n}^{(2)}d_{23n}(r)+\right.\\
\left.B_{1n}^{(2)}c_{21n}(r)+B_{2n}^{(2)}c_{22n}(r)+B_{3n}^{(2)}c_{23n}(r)\right)_{r=R-h}=0\\
\mu^{(2)}\left(A_{1n}^{(2)}d_{31n}(r)+A_{2n}^{(2)}d_{32n}(r)+A_{3n}^{(2)}d_{33n}(r)+\right.\\
\left.B_{1n}^{(2)}c_{31n}(r)+B_{2n}^{(2)}c_{32n}(r)+B_{3n}^{(2)}c_{33n}(r)\right)_{r=R-h}=0\\
\mu^{(2)}\left(A_{1n}^{(2)}d_{k1n}(r)+A_{2n}^{(2)}d_{k2n}(r)+A_{3n}^{(2)}d_{k3n}(r)+\right.\\
\left.B_{1n}^{(2)}c_{k1n}(r)+B_{2n}^{(2)}c_{k2n}(r)+B_{3n}^{(2)}c_{k3n}(r)\right)_{r=R}=\\
\mu^{(1)}\left(B_{1n}^{(1)}b_{k1n}(r)+B_{2n}^{(1)}b_{k2n}(r)+B_{3n}^{(1)}b_{k3n}(r)\right)_{r=R}\\
k=1,2,3\\
\left(A_{1n}^{(2)}d_{k1n}(r)+A_{2n}^{(2)}d_{k2n}(r)+A_{3n}^{(2)}d_{k3n}(r)+\right.\\
\left.B_{1n}^{(2)}c_{k1n}(r)+B_{2n}^{(2)}c_{k2n}(r)+B_{3n}^{(2)}c_{k3n}(r)\right)_{r=R}=\\
\left(B_{1n}^{(1)}b_{k1n}(r)+B_{2n}^{(1)}b_{k2n}(r)+B_{3n}^{(1)}b_{k3n}(r)\right)_{r=R}\\
k=4,5,6
\end{gathered} \tag{24}$$

After finding the aforementioned unknown constants from equations Eqs. (23)-(24), the Fourier transformation of the sought values is determined completely. The originals of these values are determined through calculation of the integrals given in Eq. (11) and this calculation is made numerically by employing the algorithm which is used and developed in many investigations of the first author of the present paper and his students and is detailed in the monograph by Akbarov (2015).

Note the method developed above can be called as analytic-numerical method which is employed for the solution to the 3D dynamic problem for the inhomogeneous medium. However, in the cases where the analytical solution to the mentioned dynamical problems is impossible, these problems can be solved through numerical methods such as detailed in the monograph by Atluri and Shen (2002) and in the paper by Useche and Alvarez (2016) and others listed therein.

4. Numerical results and discussions

In the present section, first we consider the algorithm for determination of the critical velocity and the algorithm for numerical calculation of the integrals in Eq. (11) for determination of the interface stresses. Further, we analyze numerical results on the critical velocity of the moving load and on the response of the interface stresses to the problem parameters, such as the velocity of the moving load, mechanical and geometrical parameters of the constituents of the system under consideration etc.

4.1 Algorithm for determination of the critical velocity

As noted above, the unknowns $A_{20}^{(2)}$, $A_{30}^{(2)}$, $B_{20}^{(2)}$, $B_{30}^{(2)}$, $B_{20}^{(1)}$ and $B_{30}^{(1)}$ are determined from the complete system of equations in Eq. (23) and below the determinant of the matrix the elements of which are the coefficients of the unknowns in these equations, is denoted through $D_0(R,h/R,\mu^{(1)}/\mu^{(2)},s,V)$.

Moreover, it can be noted that, according to the solution procedure discussed in the previous section, the unknowns $B_{1n}^{(1)}$, $B_{2n}^{(1)}$, $B_{3n}^{(1)}$, $A_{1n}^{(2)}$, $A_{2n}^{(2)}$, $A_{3n}^{(2)}$, $B_{1n}^{(2)}$, $B_{2n}^{(2)}$ and $B_{3n}^{(2)}$ for each selected n are determined from the complete system of equations in Eq. (24) and below the determinant of the matrix, the elements of which are the coefficients of the unknowns in these equations, is denoted through $D_n(R,h/R,\mu^{(1)}/\mu^{(2)},s,V)$.

If the Fourier transformation parameter s is taken as the wavenumber and the load moving velocity V as the wave propagation velocity, then the equation

$$D_0(R,h/R,\mu^{(1)}/\mu^{(2)},s,V)=0 \tag{25}$$

coincides with the dispersion equation of the longitudinal axisymmetric wave, and the equation

$$D_n(R,h/R,\mu^{(1)}/\mu^{(2)},s,V)=0 \tag{26}$$

coincides with the dispersion equation of the flexural waves for the $n-th$ harmonic in the system under consideration. The solutions to the equations Eqs. (25)-(26) can be denoted through $V_0=V_0(s)$ and $V_n=V_n(s)$, respectively, which are obtained for each fixed value of the problem parameters.

We introduce the following notation

$$\frac{\sigma_{rrF0}^{(1)}(R,s)}{\mu^{(1)}}=B_{20}^{(1)}b_{120}(R)+B_{30}^{(1)}b_{130}(R) \tag{27}$$

$$\frac{\sigma_{rrFn}^{(1)}(R,s)}{\mu^{(1)}}=B_{1n}^{(1)}b_{11n}(R)+B_{2n}^{(1)}b_{12n}(R)+B_{3n}^{(1)}b_{13n}(R) \tag{28}$$

through which, according to the first expression in Eq. (19), the Fourier transform $\sigma_{rrF}(R,\theta,s)=\sigma_{rrF}^{(1)}(R,\theta,s)=\sigma_{rrF}^{(2)}(R,\theta,s)$ of the interface normal stress $\sigma_{rr}(R,\theta,z)=\sigma_{rr}^{(1)}(R,\theta,z)=\sigma_{rr}^{(2)}(R,\theta,z)$ can be presented as follows.

$$\sigma_{rrF}(R,\theta,s)=\sigma_{rrF0}^{(1)}(R,s)+\sum_{n=1}^{\infty}\sigma_{rrFn}^{(1)}(R,s)\cos(n\theta) \tag{29}$$

Thus, after the foregoing preparation, denoting the critical velocity through V_{cr}, we can formulate the criterion for determination of this velocity as follows

$$\left|\sigma_{rr}^{(1)}(R,z,\theta)\right|\to\infty \quad \text{as} \quad V\to V_{cr} \tag{30}$$

Note that it can also be written in criterion Eq. (30) any quantities related to the stress-strain state in the constituents instead of the interface stress $\sigma_{rr}^{(1)}(R,\theta,z)$. Here, for concretization of the discussion this criterion is formulated through the stress $\sigma_{rr}^{(1)}(R,\theta,z)$.

Now, considering the dispersion curves of the axisymmetric and flexural waves, the equations of which can be presented as $V_0=V_0(s)$ and $V_n=V_n(s)$, respectively we can make the following remarks.

If there exists the case where $dV_0(s)/ds=0$ then the velocity corresponding to this case can be taken as the critical velocity (denote this critical velocity by V_{0cr}) under which

$$\left|\int_0^{+\infty}\sigma_{rrF0}^{(1)}(R,s)\cos(sz)ds\right|\to\infty \Rightarrow \left|\sigma_{rr}^{(1)}(R,\theta,z)\right|\to\infty \quad \text{as} \quad V\to V_{0cr} \tag{31}$$

takes place. If there exists the case where $dV_n(s)/ds=0$ then the velocity corresponding to this case can also be taken as the critical velocity (denoted by V_{ncr}) under which

$$\left|\int_0^{+\infty}\sigma_{rrFn}^{(1)}(R,s)\cos(sz)ds\right|\to\infty \Rightarrow \left|\sigma_{rr}^{(1)}(R,\theta,s)\right|\to\infty \quad \text{as} \quad V\to V_{ncr} \tag{32}$$

takes place.

Numerical results show that, as usual, the case Eq. (32) occurs only under n=1 and therefore the following relation can be written instead of Eq. (32).

$$\left|\int_0^{+\infty}\sigma_{rrF1}^{(1)}(R,s)\cos(sz)ds\right|\to\infty \Rightarrow \left|\sigma_{rr}^{(1)}(R,\theta,z)\right|\to\infty, \text{ as } V\to V_{1cr} \tag{33}$$

The critical velocity V_{1cr} determined from the criterion Eq. (33) appears as a result of the non-axisymmetric nature of the moving load, however, the critical velocity V_{0cr} determined from the criterion Eq. (31) relates to the corresponding axisymmetric moving load. Consequently, comparison of the values of the critical velocities V_{0cr} and V_{1cr} can resolve "whether the values of the critical speed of the moving load depend on the non-axisymmetricity of this load or whether the critical velocity determined for the corresponding axisymmetric moving load case also occurs for the non-axisymmetric moving load case". Consequently, if $V_{0cr}<V_{1cr}$ then the minimum critical velocity of the non-axisymmetric moving load is the same as in the corresponding axisymmetric moving load, however, if $V_{1cr}<V_{0cr}$ then the non-axisymmetricity of the moving load causes the minimum critical velocity to decrease. Note that the criteria Eq. (31) and Eq. (33) can also be employed without consideration of the dispersion curves obtained from the solution of the equations Eqs. (25)-(26). Thus, the aforementioned critical velocities can also be determined by direct calculation of the values $\left|\sigma_{rr}^{(1)}(R,\theta,z)\right|$ through the corresponding integrals in Eq. (11) for various values of the moving load velocity V. For determination of the critical velocity, the latter approach is more general than that based on the dispersion curves and can be employed not only for the cases where the constituents of the system are purely elastic, but also for the cases where these materials are time-dependent.

This completes the consideration of the algorithm for calculation of the critical velocity.

4.2 Algorithm for calculation of the integrals in (Eq. (11))

Here, this algorithm is explained with respect to the calculation of the values of the interface normal stress $\sigma_{rr}(R, \theta, z)$, the Fourier transformation of which is determined through the expression Eq. (29). According to the integrals in Eq. (11) and according to the equation Eq. (29), we can write the following approximate expression for this stress.

$$\begin{aligned}\sigma_{rr}(R,\theta,z) &= \int_0^{+\infty} \sigma_{rrF}(R,\theta,s)\cos(sz)\mathrm{d}s \\ &\approx \int_0^{+\infty} \sigma_{rrF0}^{(1)}(R,s)\cos(sz)\mathrm{d}s + \\ &\sum_{n=1}^{N}\left(\int_0^{+\infty} \sigma_{rrFn}^{(1)}(R,s)\cos(sz)\mathrm{d}s\right)\cos(n\theta)\end{aligned} \tag{34}$$

In relation Eq. (34) the infinite Fourier series is replaced by the corresponding finite one and the number of terms in this finite series, i.e., the number N in Eq. (34) is determined from the convergence requirement of the numerical results.

The integrals in Eq. (34) and as well as in Eq. (11) are called the wavenumber integrals and, according to the dispersion equations Eqs. (25)-(26), the integrated functions have singular points with respect to s and if the order of this singularity is equal to one, then the integrals have a meaning in Cauchy's principal value sense. However, in the cases where the order of the singularity is equal to two, then these cases cause resonance type behaviour. As, under calculation of the integrals, we consider the cases where $0<V<\min(V_{0cr};V_{1cr})$ and therefore, the order of all the singular points is one for this interval of the moving load velocity and only in the cases where $V=V_{0cr}$ or $V=V_{1cr}$ does the order of this singularity become two.

Thus, as a result of the existence of the noted singularities, calculation of the wavenumber integrals requires a special algorithm which is detailed in the works by Akbarov (2015), Jensen *et al*. (2011) and others listed therein. It should be noted that among these algorithms a more suitable and convenient one is the algorithm based on the use of the Sommerfeld contour and for employing this algorithm, according to Cauchy's theorem, the contour $[0,+\infty]$ is "deformed" into the contour C (Fig. 2), which is called the Sommerfeld contour in the complex plane $s = s_1 + \mathrm{i}s_2$ and in this way the real roots of the equations Eqs. (25)-(26) are avoided.

Despite this avoidance, the values of the integrals calculated by the Sommerfeld contour algorithm have a jump in the near vicinity of the second order singular points. Such cases, which appear with respect to the concrete problems as examples, are also detailed in the monograph by Akbarov (2015). Hence, this method also allows for determination of the critical velocity through direct calculation of the stress $\sigma_{rr}^{(1)}(R,\theta,s)$ which enters into the criteria Eqs. (32)-(33), and determines the critical

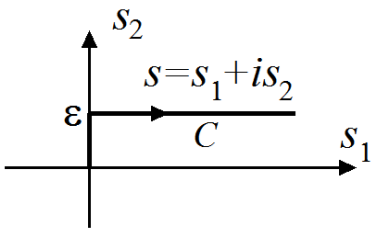

Fig. 2 The sketch of the Sommerfeld contour

velocities without using the solution to the dispersion equations Eqs. (25)-(26).

Thus, according to the foregoing discussions, the integrals in Eq. (34) can be presented as follows.

$$\begin{aligned}\sigma_{rr}(R,\theta,z) &= \int_C \sigma_{rrF}(R,\theta,s)\cos(sz)\mathrm{d}s \\ &= \int_C \sigma_{rrF0}^{(1)}(R,s)\cos(sz)\mathrm{d}s + \\ &\sum_{n=1}^{N}\left(\int_C \sigma_{rrFn}^{(1)}(R,s)\cos(sz)\mathrm{d}s\right)\cos(n\theta)\end{aligned} \tag{35}$$

Using the configuration of the contour C given in Fig. 2 we can write the following relation for the integrals in Eq. (35).

$$\begin{aligned}&\int_C f(s)\cos(sz)\mathrm{d}s \\ &= \int_0^{+\infty} f(s_1+\mathrm{i}\varepsilon)\cos((s_1+\mathrm{i}s)z)\mathrm{d}s_1 + \int_0^{\varepsilon} f(\mathrm{i}s_2)\mathrm{d}s_2\end{aligned} \tag{36}$$

Assuming that $\varepsilon<<1$, the last integral in Eq. (36) can be neglected and we can use the following expressions for calculation of the stress $\sigma_{rr}(R,\theta,z)$.

$$\begin{aligned}\sigma_{rr}(R,\theta,z) &\approx \int_0^{+\infty} \sigma_{rrF}(R,\theta,s_1+\mathrm{i}\varepsilon)\cos((s_1+\mathrm{i}\varepsilon)z)\mathrm{d}s_1 \\ &= \int_0^{+\infty} \sigma_{rrF0}^{(1)}(R,s_1+\mathrm{i}\varepsilon)\cos((s_1+\mathrm{i}\varepsilon)z)\mathrm{d}s_1 + \\ &\sum_{n=1}^{N}\left(\int_0^{+\infty} \sigma_{rrFn}^{(1)}(R,s_1+\mathrm{i}\varepsilon)\cos((s_1+\mathrm{i}\varepsilon)z)\mathrm{d}s_1\right)\cos(n\theta)\end{aligned} \tag{37}$$

Under calculation procedure, the improper integrals $\int_0^{+\infty} f(\bullet)\mathrm{d}s_1$ in Eq. (37) are replaced with the corresponding definite integrals $\int_0^{+S_1^*} f(\bullet)\mathrm{d}s_1$ and the values of S_1^* are defined from the corresponding convergence requirement.

Moreover, under calculation of these definite integrals, the interval $\left[0, S_1^*\right]$ is divided into a certain number (denote this number through N_1) of shorter intervals and within each of these shorter intervals, the integrals are calculated by the use of the Gauss algorithm with ten

integration points. The values of the integrated functions at these integrated points are determined through the solution of the Eqs. (23)-(24). All these procedures are performed automatically in the PC by use of the corresponding programs constructed by the authors of the paper in MATLAB.

Finally, note that the testing of the algorithms described above has been made in many investigations by the authors (see, for instance, the works by Akbarov (2015) and by Akbarov and Mehdiyev (2017) and others listed therein) and therefore this testing is not illustrated again here. At the same time, it must be noted that the all numerical results which will be discussed below are obtained in the case where N_1=200, $S_1^* = 9$ and ε=0.001. However, examples on the convergence of the numerical results with respect to the number N in Eq. (37) (i.e., with respect to the terms in the finite Fourier series) will be given below.

This completes the consideration of the algorithm for calculation of the integrals in Eq. (11).

4.3 Numerical results related to the critical velocity

Numerical results are obtained for the following selected material properties of the constituents of the system under consideration.

$$\text{Case 1.}\quad E^{(1)}/E^{(2)} = 0.35,\ \rho^{(1)}/\rho^{(2)} = 0.1,\ \nu^{(1)} = \nu^{(2)} = 0.25 \tag{38}$$

$$\text{Case 2.}\quad E^{(1)}/E^{(2)} = 0.05,\ \rho^{(1)}/\rho^{(2)} = 0.01,\ \nu^{(1)} = \nu^{(2)} = 0.25 \tag{39}$$

$$\text{Case 3.}\quad E^{(1)}/E^{(2)} = 0.5,\ \rho^{(1)}/\rho^{(2)} = 0.5,\ \nu^{(1)} = \nu^{(2)} = 0.3 \tag{40}$$

$$\text{Case 4.}\quad E^{(1)}/E^{(2)} = 0.02,\ \rho^{(1)}/\rho^{(2)} = 0.01,\ \nu^{(1)} = \nu^{(2)} = 0.25 \tag{41}$$

$$\text{Case 5.}\quad E^{(1)}/E^{(2)} = 0.01,\ \rho^{(1)}/\rho^{(2)} = 0.01,\ \nu^{(1)} = \nu^{(2)} = 0.25 \tag{42}$$

The values of the critical velocities obtained in the foregoing cases under various values of the ratio h/R are given in Table 1. Note that Case 2 is also considered in the paper by Abdulkadirov (1981) and the critical velocity $V_{0cr}/c_2^{(2)}$ is determined only for the case where $h/R = 0.5$. The value of $V_{0cr}/c_2^{(2)}$ determined in the paper by Abdulkadirov (1981) is also given in the corresponding box in Table 1 from which follows that in the indicated particular case, the present result coincides with the corresponding result obtained in the paper by Abdulkadirov (1981) with very high accuracy. Moreover, Case 3 is also considered in the paper Babich *et al*. (1986) under determination of the critical velocity of the moving load acting on the stratified half-plane. According to the well-known mechanical consideration, in Case 3 the results obtained in the present case and related to $V_{0cr}/c_2^{(2)}$ must approach the corresponding results obtained in the paper by Babich, Glukhov and Guz (1986) which are also given in the corresponding box in Table 1 as $h/R \to 0$. Analysis of the results obtained in Case 3 and given in Table 1, proves the foregoing prediction. Consequently, the two aforementioned comparisons of the present results with the known ones obtained by other researchers illustrate the validity and reliability of the calculation algorithm and PC programs used.

Table 1 The values of the dimensionless critical velocities $V_{0cr}/c_2^{(2)}$ (upper number) and $V_{1cr}/c_2^{(2)}$ (lower number) for various values of the ratio h/R and for cases indicated in Eqs. (38)-(42)

h/R	Cases				
	Case 1	Case 2	Case 3	Case 4	Case 5
0.5	0.9355	0.8261 (*)	0.9396	0.8052	0.7977
	0.9405	0.7773	0.9432	0.6250	0.5178
0.4	0.9108	0.7670	0.9184	0.7400	0.7303
	0.9196	0.7540	0.9296	0.6524	0.5439
0.3	0.8865	0.6977	0.8918	0.6615	0.6483
	0.8886	0.6950	0.9042	0.6536	0.5800
0.2	0.8642	0.6176	0.8743	0.5663	0.5470
	0.8683	0.6196	0.8785	0.5652	0.5443
0.1	0.8437	0.5291	0.8547	0.4490	0.4157
	0.8453	0.5316	0.8565	0.4504	0.4163
0.05	0.8360	0.4885	0.8470	0.3838	0.3341
	0.8365	0.4898	0.8475	0.3849	0.3349
0.01	0.8315	0.4683	0.8423 (**)	0.3442	0.2738
	–	0.4684	0.8423	0.3443	0.2739

(*): 0.826 by Abdulkadirov (1981)
(**): 0.832 by Babich *et al*. (1986)

It follows from Table 1 that the values of $V_{0cr}/c_2^{(2)}$ and $V_{1cr}/c_2^{(2)}$ decrease with decreasing of the ratio h / R and the values of $V_{0cr}/c_2^{(2)}$ and $V_{1cr}/c_2^{(2)}$ approach to each other as $h/R \to 0$. This can be explained as follows.

As noted above, the critical velocity $V_{0cr}/c_2^{(2)}$ approaches the critical velocity obtained for the corresponding plane strain state as $h/R \to 0$. At the same time, according to the well-known mechanical consideration, the critical velocity $V_{1cr}/c_2^{(2)}$ approaches the critical velocity obtained for the corresponding 3D problem on the point-located moving load acting on the "plate+half-space" system. In the paper Akbarov *et al*. (2015), it is established that the critical velocity obtained in the noted 3D case coincides with the critical velocity obtained for the corresponding plane-strain state. Namely, with this fact the approaching of the critical velocities

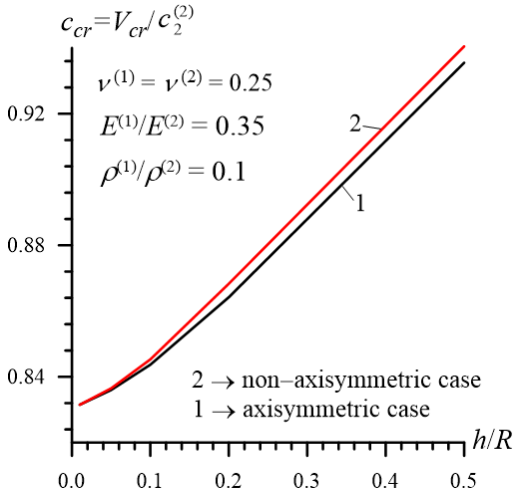

(a) in Case 1 (Eq. (38))

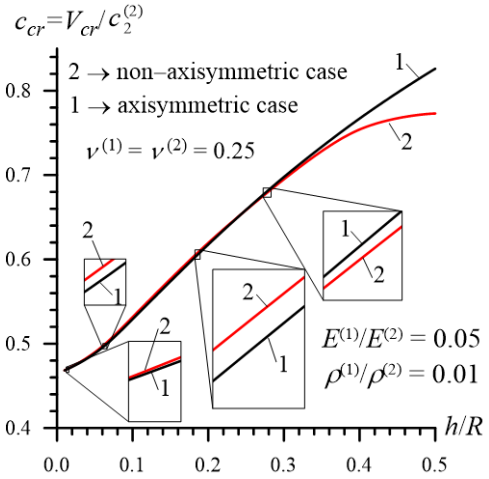

(b) in Case 2 (Eq. (39))

Fig. 2 The sketch of the Sommerfeld contour

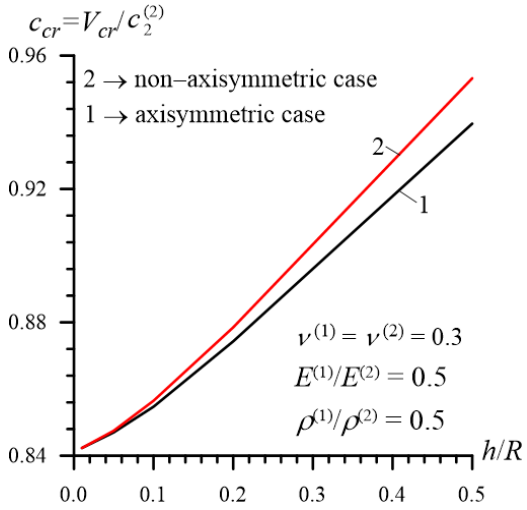

(a) in Case 3 (Eq. (40))

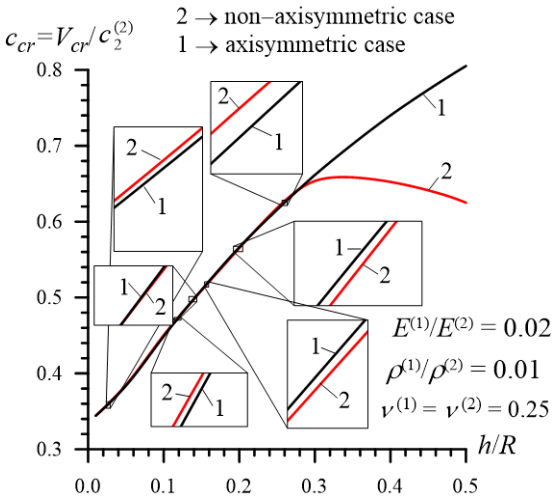

(b) in Case 4 (Eq. (41))

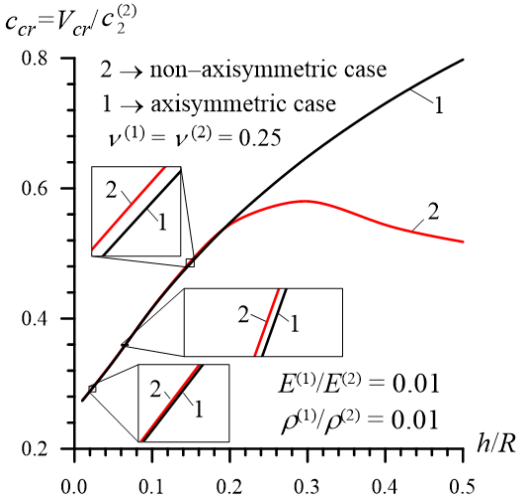

(c) in Case 5 (Eq. (42))

Fig. 3 Dependence between the critical velocity and the ratio h/R

$V_{0cr}/c_2^{(2)}$ and $V_{1cr}/c_2^{(2)}$ to each other as $h/R\to 0$, is explained. This fact can also be taken as validation of the obtained numerical results.

Using the comparison of the values of the critical velocity $V_{0cr}/c_2^{(2)}$ with the corresponding ones of the critical velocity $V_{1cr}/c_2^{(2)}$, we can make concrete conclusions on the influence of the non axisymmetricity of the moving load on the critical velocity. For a clearer illustration of this comparison, we use the graphs given in Fig. 3, which show dependencies among $V_{0cr}/c_2^{(2)}$, $V_{1cr}/c_2^{(2)}$ and h/R in Case 1 Fig. 3(a), Case 2 Fig. 3(b) Case 3 Fig. 3(c), Case 4 Fig. 3(d) and Case 5 Fig. 3(e). In Fig. 3 the graphs indicated by the number 1 (by the number 2) relate to the dependence between $V_{0cr}/c_2^{(2)}$ and h/R (between $V_{1cr}/c_2^{(2)}$ and h/R).

Thus, it follows from the analysis of Fig. 3 that for the considered change range of the ratio h/R in all the cases shown in Eqs. (38)-(42), the values of $V_{0cr}/c_2^{(2)}$ increase monotonically with increasing of the ratio h / R and this conclusion occurs also for $V_{1cr}/c_2^{(2)}$ in Case 1, in Case 2 and in Case 3. However, in Case 4 and in Case 5,

the dependence between $V_{1cr}\big/c_2^{(2)}$ and h/R has a non-monotonic character. Moreover, it follows from Fig. 3 that in Case 1 and in Case 3, the inequality $V_{0cr}<V_{1cr}$ takes place. However, in Case 2, in Case 4 and in Case 5, this inequality occurs before a certain value of the ratio h/R (denote it by$(h/R)^*$), however, in the cases where $h/R>(h/R)^*$ the inequality $V_{1cr}<V_{0cr}$ occurs.

Comparison of the results obtained in Case 2, in Case 4 and in Case 5 with each other shows that the values of $(h/R)^*$ decrease with decreasing of the ratio $E^{(1)}/E^{(2)}$, i.e., with increasing of the modulus of elasticity $E^{(2)}$ of the cylinder material under a fixed value of the modulus of elasticity $E^{(1)}$ of the surrounding elastic medium.

Moreover, in Case 2, in Case 4 and in Case 5 the values of $(V_{0cr}-V_{1cr})$ increase with h/R under $h/R>(h/R)^*$.

This completes the analysis of the numerical results related to the critical velocity and, according to this analysis, the following main conclusion can be made: the non axisymmetricity of the moving load acting in the interior of the hollow cylinder surrounded with elastic medium can decrease significantly the values of the critical velocity of this load. Moreover, these results show that the non axisymmetricity of the moving load can change the critical velocity of the moving load not only in the quantitative sense but also in the qualitative sense: the examples for which are the dependencies between the critical velocity and the ratio h/R obtained in Case 2, in Case 4 and in Case 5.

4.4 Numerical results related to the interface stresses

Here, only the numerical results which relate to Case 4 (Eq. (41)) are considered, and the corresponding results obtained for the other cases indicated in Eqs. (38)-(40) and Eq. (42) in the qualitative sense are similar with those obtained in Case 4. These results relate to the response of the interface normal stress $\sigma_{rr}(R,\theta,z)$ and the shear stresses $\sigma_{rz}(R,\theta,z)$ and $\sigma_{r\theta}(R,\theta,z)$, where

$$\begin{aligned}
&\sigma_{rr}(R,\theta,z)=\sigma_{rr}^{(1)}(R,\theta,z)=\sigma_{rr}^{(2)}(R,\theta,z)\\
&\sigma_{rz}(R,\theta,z)=\sigma_{rz}^{(1)}(R,\theta,z)=\sigma_{rz}^{(2)}(R,\theta,z)\\
&\sigma_{r\theta}(R,\theta,z)=\sigma_{r\theta}^{(1)}(R,\theta,z)=\sigma_{r\theta}^{(2)}(R,\theta,z)
\end{aligned} \tag{43}$$

to the load moving velocity $c=V/c_2^{(2)}$ in the cases where $V<\min\{V_{0cr};V_{1cr}\}$, to the ratio h/R and to the angle α within which the external load is distributed uniformly. Moreover, we consider the distribution of these stresses with respect to the coordinates z and θ. At the same time, at the end of the subsection, for illustration of the influence of the ratio of the modulus of elasticity of the constituents on the foregoing interface stresses, some numerical results related to Case 2 and to Case 5 are also considered.

The results illustrated in Fig. 4 show the convergence of the numerical results related to the stress $\sigma_{rr}(R,\theta,z)$ at $\{\theta=0;\ z=0\}$ obtained for various values of the dimensionless

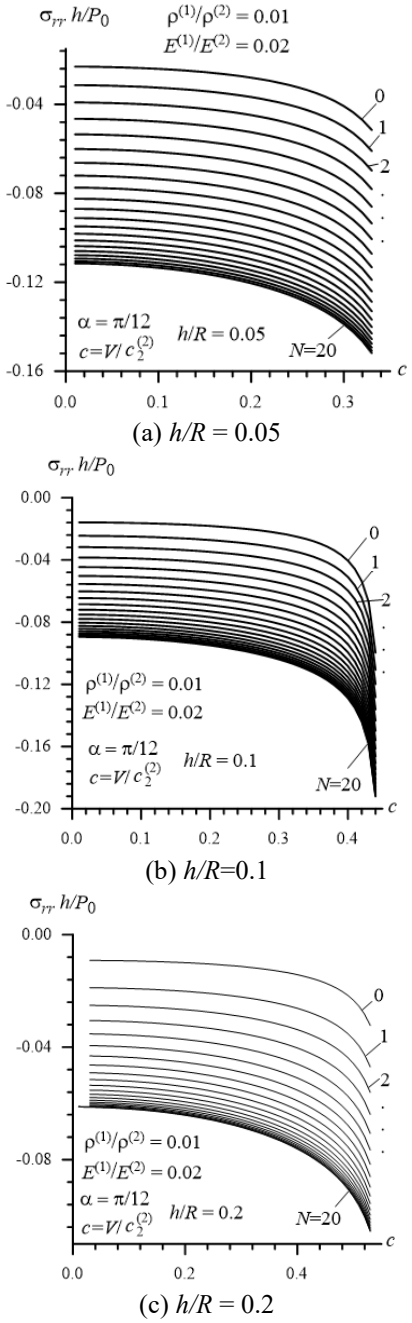

(a) $h/R = 0.05$

(b) h/R=0.1

(c) $h/R = 0.2$

Fig. 4 Convergence of the normal stress values with respect to the number N in the Fourier series presentation of this stress

moving velocity $c\,(=V/c_2^{(2)})$ in the cases where h/R=0.05 Fig. 4(a), 0.1 Fig. 4(b) and 0.2 Fig. 4(c) under $\alpha=\pi/12$, with respect to the number N in the Fourier series presentation of the sought values such as in Eq. (35). It follows from these results that the aforementioned convergence improves with the ratio h/R and it is enough to take N=15 in the series presentation in order to obtain results with an accuracy which is not less than 10^{-4}. Therefore, in the present investigation all the numerical results are obtained in the case where N=15 in the series presentation of the sought values. Below, other examples of the convergence of the numerical results with respect to the

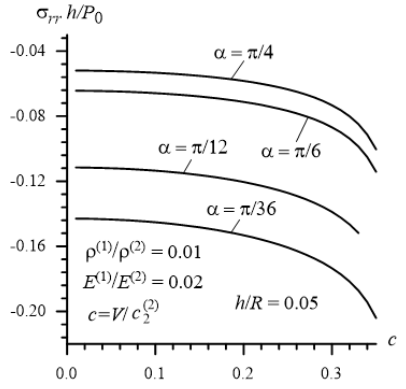

(a) $h/R = 0.05$

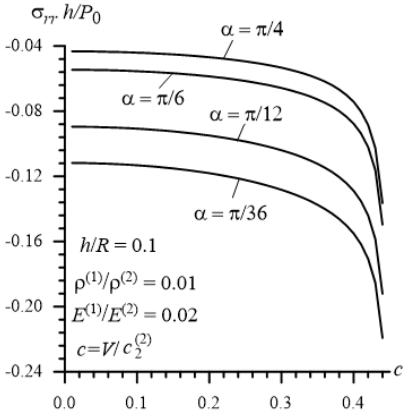

$h/R = 0.1$

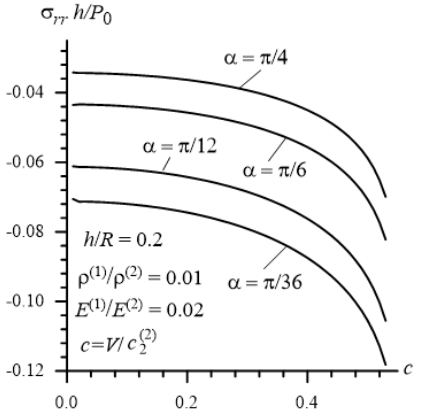

(c) $h/R = 0.2$

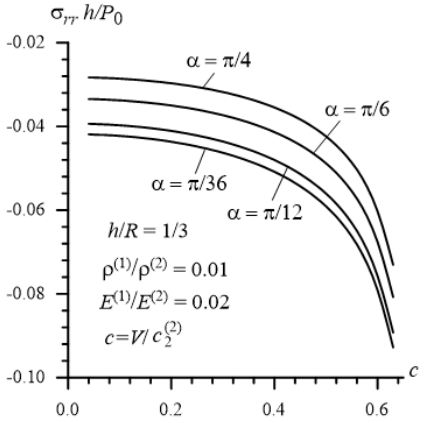

(d) h/R=1/3

Fig. 5 The influence of the angle α on the response of the normal stress to the load moving velocity

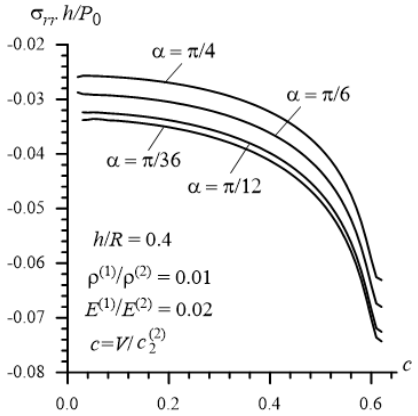

(e) h/R=0.4

Fig. 5 Continued

number N will also be considered.

The graphs given in Fig. 5 show the response of the normal stress $\sigma_{rr}(R,\theta,z)$ at $\{\theta=0; z=0\}$ to the dimensionless velocity of the moving load in the cases where h/R=0.05 Fig. 5(a), 0.1 Fig. 5(b), 0.2 Fig. 5(c), 1/3 Fig. 5(d) and 0.4 Fig. 5(e) for various values of the angle α Fig. 1(b). It follows from these graphs that in the all considered values of the ratio h/R, an increase in the angle α causes a decrease in the absolute values of the interface normal stress. Moreover, it follows from these graphs that the absolute values of the stress increase monotonically with the load moving velocity and the results obtained for various α approach each other with this velocity. This is because the values of the corresponding critical velocities do not depend on the angle α. Comparison of the results obtained for various h/R shows that the influence of the angle α on the values of the stress becomes more considerable with decreasing of the ratio h/R.

For a clearer illustration of the influence of the ratio h/R on the values of the stress we consider the graphs of the dependence between $\sigma_{rr}(R,0,0)$ and c constructed for various h/R under a fixed angle α. Fig. 6 shows such types of graphs which are obtained in the cases where $\alpha=\pi/36$ Fig. 6(a), $\alpha=\pi/12$ Fig. 6(b) and $\alpha=\pi/6$ Fig. 6(c). Thus, according to these graphs it can be concluded that an increase in the ratio h/R causes a significant decrease in the absolute values of the stress $\sigma_{rr}(R,0,0)$.

The distributions of the stress σ_{rr} at $\theta=0$ with respect to the dimensionless coordinate z/h are given in Fig. 7 which are constructed in the cases where h/R=0.05 (Fig. 7(a), c=0.35), 0.1 (Fig. 7(b), c=0.40) and 0.2 (Fig. 7(c), c=0.40) under various values of the angle α. These results show that the values of the stress decay with the distance from the point z/h=0 at which the moving load acts. Moreover, these results also show that under h/R≤0.1 at a certain distance from the point at which the moving load acts both behind and ahead of this point, the interface normal stress becomes a stretched one. Note that this moment can play an important role in the adhesion strength of the "hollow cylinder+surrounding elastic medium" system.

Moreover, the following statement should be noted. For this purpose, we recall that that the coordinate z with

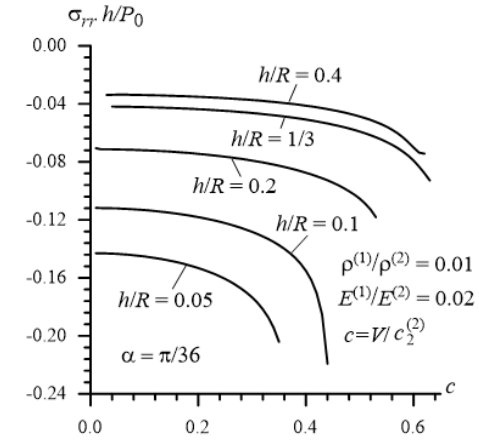

(a) $\alpha=\pi/36$

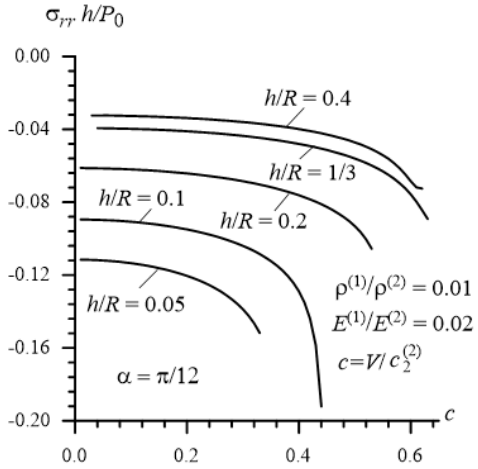

(b) $\pi/12$

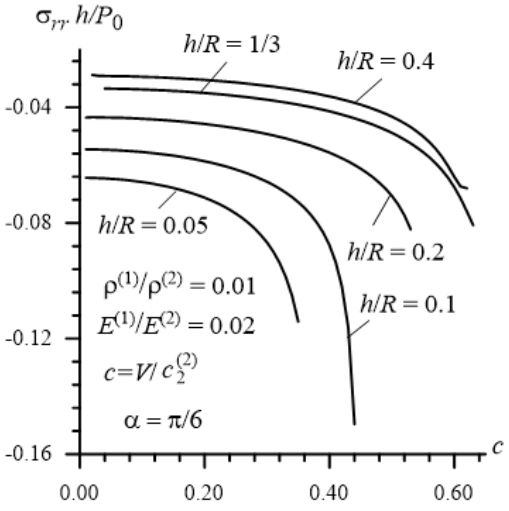

(c) $\pi/6$

Fig. 6 The influence of the ratio on the response of the normal stress to the load moving velocity

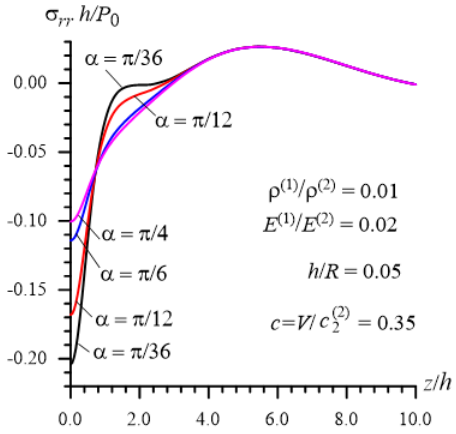

(a) h/R=0.05

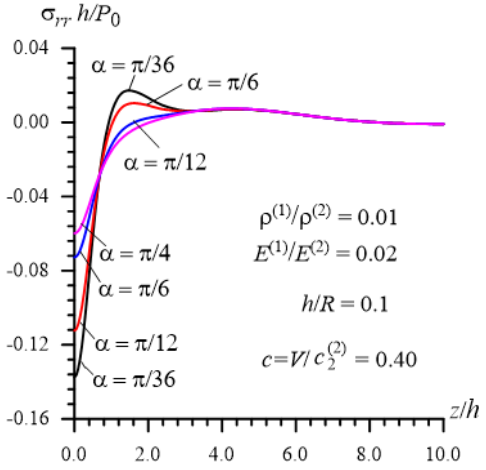

(b) h/R=0.1

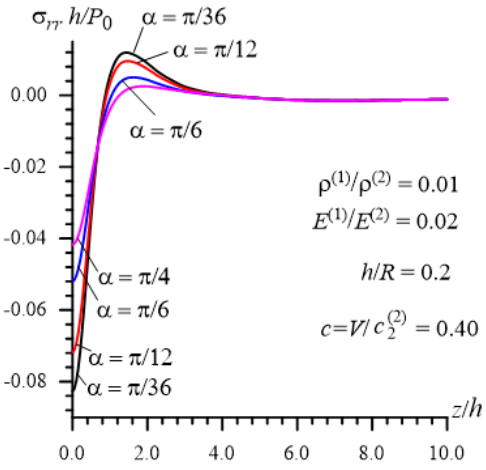

(c) h/R=0.2

Fig. 7 Distribution of the normal stress with respect to the dimensionless coordinate z/h

respect to which the distribution of the interface normal stress is illustrated in Fig. 7, and others which will be given below for the interface shear stresses σ_{rz} and $\sigma_{r\theta}$ (43), is the coordinate in the moving coordinate system determined by the expressions in Eq. (10), i.e., the z/h in these figures is the z'/h. Consequently, for a more correct explanation of the results given in Fig. 7 and other corresponding ones given below, for the interface shear stresses we must take into consideration the $(z-Vt)/h$ (where z is the coordinate in the reference coordinate system) instead of z/h. According to this consideration, if the time t(=t*) is fixed, then these figures illustrate the distribution of the stresses with respect to the spatial coordinate (z'=z−Vt*) which shows the distance in the cylinder's axis direction from the point at

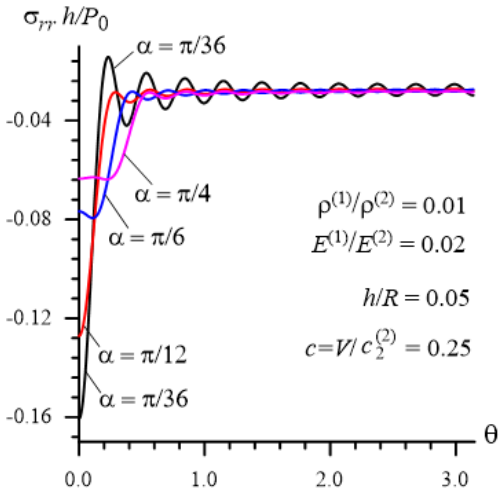

(a) h/R=0.05

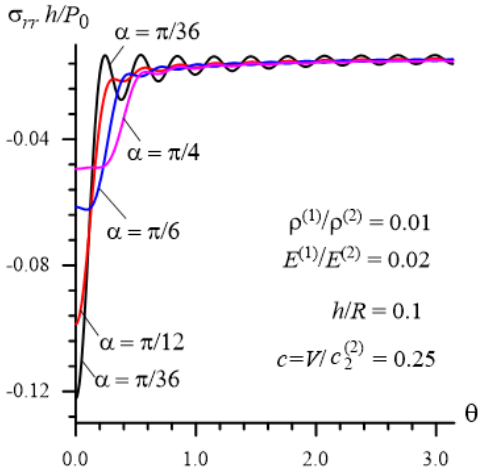

(b) h/R=0.1

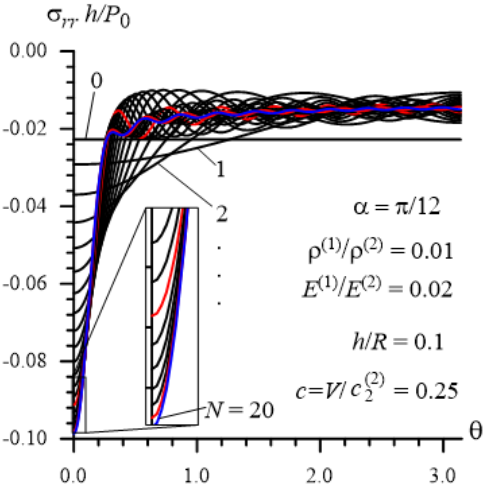

(c) Convergence of the distribution with respect to the number N in the Fourier series presentation of this stress in the cases where $\alpha=\pi/12$

Fig. 8 Distribution of the normal stress with respect to the coordinate θ

which the moving load acts. If the spatial coordinate z=z* is fixed in the reference coordinate system, then, according to (z'=z*−Vt), Fig. 7 and the other corresponding ones given

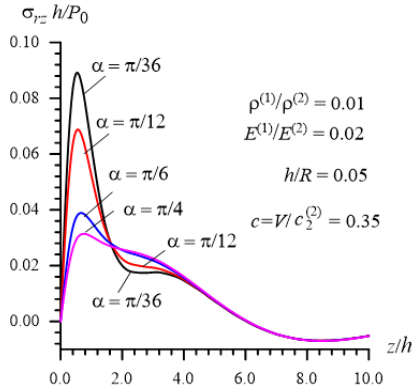

(a) h/R=0.05

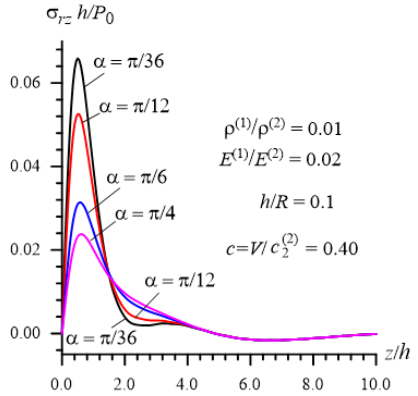

(b) h/R=0.1

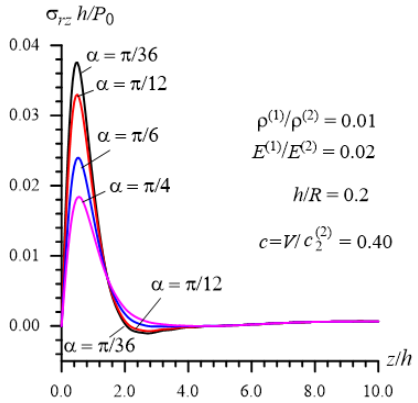

(c) h/R=0.2

Fig. 9 Distribution of the shear stress σ_{rz} with respect to the dimensionless coordinate z/h

below illustrate the change of the stresses with respect to time at the fixed point mentioned. Consequently, the results given in Fig. 7 and the other corresponding ones given below (see, Figs. 9-10) illustrate not only the distribution of the interface stresses with respect to the spatial coordinate, but also the change of these stresses with respect to time.

The distribution of the normal stress σ_{rr} at z/h=0 with respect to the circumferential coordinate θ for various angles α under c=0.25 is given in Figs. 8(a)-(b) for the cases where h/R=0.05 and 0.1 respectively. It follows from the analysis of the graphs given in Figs. 8(a) and 8(b) that in the cases where $\alpha=\pi/36$ and $\alpha=\pi/12$, the absolute maximum value of the normal stress appears at θ=0, however, in the cases where $\alpha=\pi/6$ and $\alpha=\pi/4$ the absolute maximum value

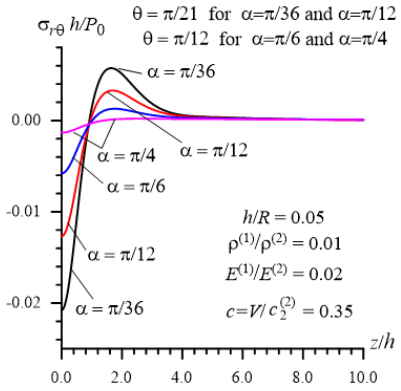

(a) h/R=0.05

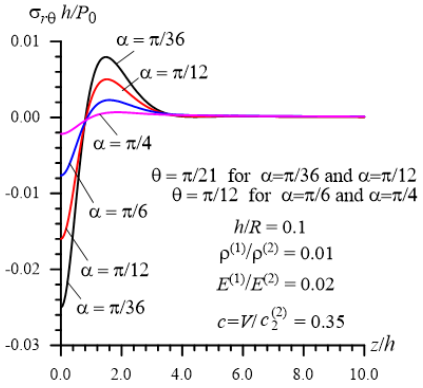

(b) h/R=0.1

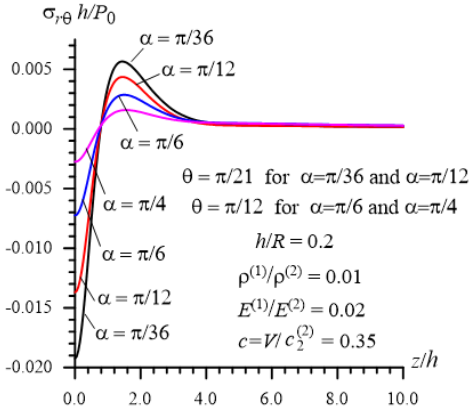

(c) h/R=0.2

Fig. 10 Distribution of the shear stress $\sigma_{r\theta}$ with respect to the dimensionless coordinate

of the stress appears at $\theta=\theta^*>0$.

The results given in Fig. 8(c) which are obtained for the cases where $\alpha=\pi/12$ and h/R=0.1, respectively illustrate the convergence of the considered dependence with respect to the number N in the Fourier series presentation of the normal stress Eq. (37). It follows from these results that in the case where $\alpha=\pi/12$, for each value of N in the near vicinity of the point $\theta=0$, the dependence between the stress and θ is monotonic.

Numerical results, which are not given here, show that the response of the shear stresses σ_{rz} and $\sigma_{r\theta}$ to the load moving velocity is similar in the qualitative sense with the results which are obtained for the normal stress σ_{rr} which are discussed above and therefore, we do not consider the

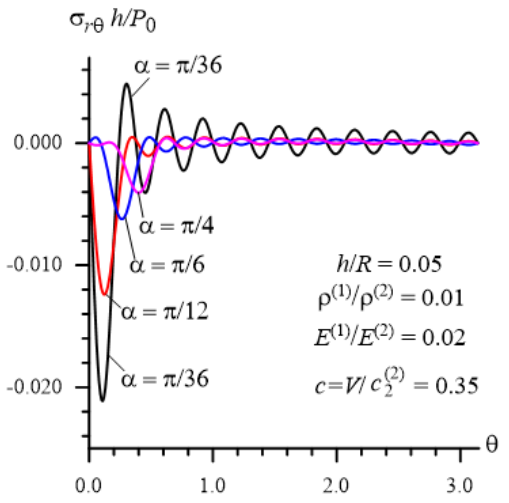

(a) h/R=0.05

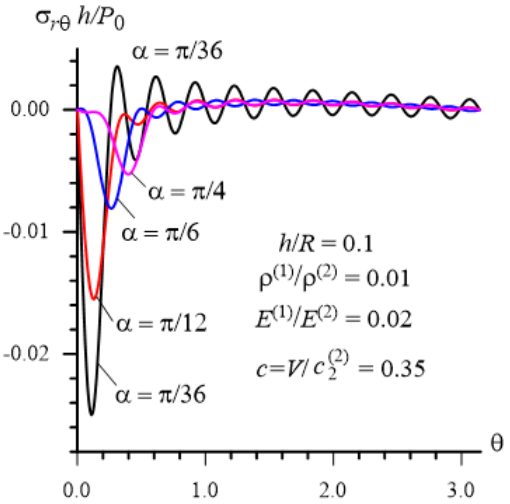

(b) h/R=0.1

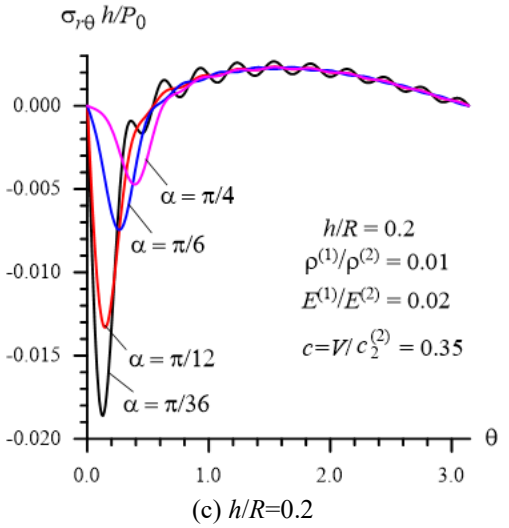

(c) h/R=0.2

Fig. 11 Distribution of the shear stress $\sigma_{r\theta}$ with respect to the coordinate θ

results related to this response, here. Moreover, these numerical results show that the dependence between the shear stress σ_{rz} and θ is also similar in the qualitative sense with the results obtained for the corresponding dependence

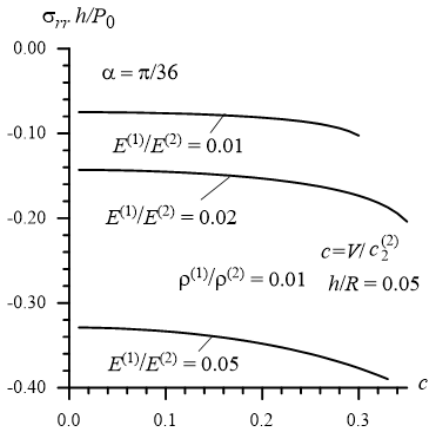

(a) $\alpha=\pi/36$

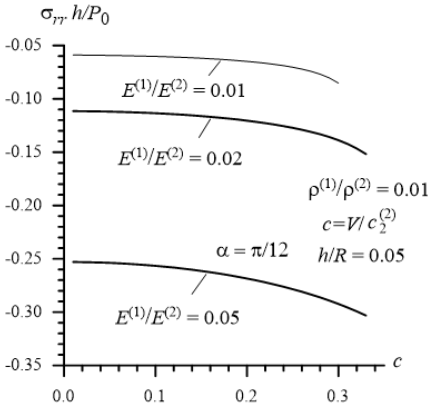

(b) $\alpha=\pi/12$

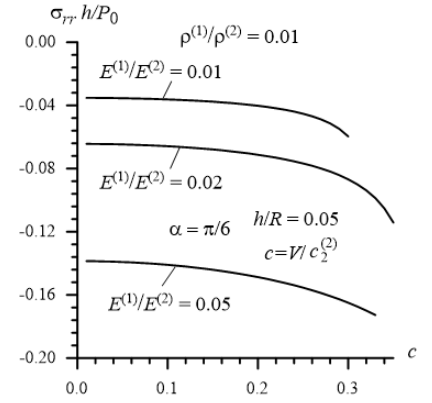

(c) $\alpha=\pi/6$

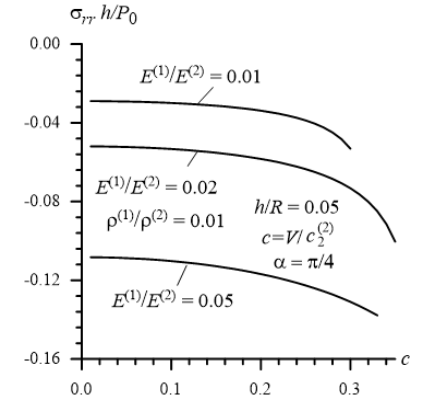

(d) $\alpha=\pi/4$

Fig. 12 The influence of the ratio modulus of elasticity of the constituents on the interface normal stress

between the normal stress σ_{rr} and θ, and therefore, this dependence for the shear stress σ_{rz} is not considered here.

Thus, taking the foregoing discussions into consideration, we consider the graphs given in Fig. 9 which show the distribution of the shear stress σ_{rz} at θ=0 with respect to the dimensionless coordinate z/h for various values of the angle α under h/R=0.05 (Fig. 9(a), for c=0.35), 0.1 (Fig. 9(b), for c=0.40) and 0.2 (Fig. 9(c), for c=0.40). It follows from Fig. 9 that the absolute values of the shear stress σ_{rz} decrease with the angle α and with the ratio h/R. Moreover, it follows from Fig. 9 that the location of the point at which the shear stress σ_{rz} has its absolute maximum depends significantly on α and h/R.

The distribution of the shear stress $\sigma_{r\theta}$ with respect to z/h is illustrated with the graphs given in Fig. 10 constructed for various values of α under c=0.35 in the cases where h/R=0.05 (Fig. 10(a)), 0.1 (Fig. 10(b)) and 0.2 (Fig. 10(c)). Analysis of these results shows that the distribution of the shear stress $\sigma_{r\theta}$ with respect to z/h is similar to that obtained for the normal stress σ_{rr}. For instance, this analysis shows that the absolute values of the shear stress $\sigma_{r\theta}$ decreases as the normal stress σ_{rr} with the ratio h/R.

However, the distribution of the shear stress $\sigma_{r\theta}$ with respect to θ at z/h=0 is not similar to that obtained for the normal stress σ_{rr}. This distribution for $\sigma_{r\theta}$ is illustrated with the graphs given in Fig. 11 which are constructed for various α under h/R=0.05 (Fig. 11(a)), 0.1 (Fig. 11(b)) and 0.2 (Fig. 11(c)) in the case where c=0.35. It follows from these graphs that the absolute maximum value of the stress $\sigma_{r\theta}$ appears at $\theta=\theta'>0$ and the values of θ' depend significantly on the angle α. Thus, the values of θ' increase with α. The other properties of the distributions given in Fig. 11 are similar to those which relate to the distribution of the other stresses considered above.

Finally, we consider the results given in Fig. 12 which illustrate the influence of the ratio of the modulus of elasticity of the constituents on the interface normal stress at $\{\theta=0; z=0\}$ in the cases where $\alpha=\pi/36$ (Fig. 12(a)), $\pi/12$ (Fig. 12(b)), $\pi/6$ (Fig. 12(c)) and $\pi/4$ (Fig. 12(d)). It follows from these results that an increase in the values of the modulus of elasticity of the cylinder material under a fixed value of the modulus of elasticity of the surrounding elastic medium or a decrease in the values of the modulus of elasticity of the surrounding elastic medium under constant value of the modulus of elasticity of the cylinder material causes a decrease in the absolute values of the interface stress. This result agrees well with the well-known mechanical and engineering considerations. Note that similar results are also obtained for the interface shear stresses.

This completes the analysis of the numerical results related to the interface stresses' distribution.

5. Conclusions

Thus, in the present paper, the non-axisymmetric 3D problem on the dynamics of the moving load acting in the interior of the hollow cylinder surrounded with elastic medium is studied by utilizing the exact equations of elastodynamics. It is assumed that in the interior of the

cylinder, a point located with respect to the cylinder axis, symmetric with respect to the vertical axis in the cross section of the cylinder and within a certain central angle α, that uniformly distributed normal and moving with constant velocity forces act. It is also assumed that the vertical component of the summation of these forces is constant and the value of this constant does not depend on the angle α, however, the horizontal component of the summation of these forces is equal to zero. The solution to the problem is based on employing the moving coordinate method, on the Fourier transform with respect to the spatial coordinate indicating the distance of the point on the cylinder axis from the point at which the moving load acts and on the Fourier series presentation of the Fourier transforms of the sought values. Each term of these series is determined analytically, however, the original terms are found numerically by employing the corresponding PC programs and algorithms. Numerical results are presented and under analyses of these results, the main attention is focused on whether the values of the critical speed of the moving load depends on the non-axisymmetricity of this load or whether the critical velocity determined for the corresponding axisymmetric moving load case occurs also for the non-axisymmetric moving load case and how the problem parameters influence the interface stresses' distribution as well as the response of these stresses to the moving load velocity. According to these analyses, the following concrete conclusions can be made:

• The non axisymmetricity of the moving load can decrease significantly the values of the critical velocity and the magnitude of this decrease depends significantly on the ratio h/R (where h is the thickness of the cylinder and R is the external radius of the cross section of the cylinder) on the ratio $E^{(1)}/E^{(2)}$ (where $E^{(1)}/(E^{(2)})$is the modulus of elasticity of the cylinder (surrounding material));

• In the relatively small values of the ratios h/R and $E^{(1)}/E^{(2)}$ (for instance in Case 1 Eq. (38) and in Case 3 Eq. (41)) under $0.01 \leq h/R \leq 0.5$ the non-axisymmetricity of the moving load does not influence the minimum critical velocity and this velocity coincides with the corresponding one obtained for the corresponding axisymmetric moving load;

• The foregoing conclusion occurs also in the relatively small values of the ratio $E^{(1)}/E^{(2)}$ (for instance, in Case 2 Eq. (39), Case 4 (41) and Case 5 Eq. (42)) before a certain value of h/R (denoted by h/R^*), however, in the cases where $h/R>(h/R)^*$ the non-axisymmetricity of the moving load causes a decrease in the values of the minimum critical velocity and the values of $(h/R)^*$ decrease with decreasing of the ratio $E^{(1)}/E^{(2)}$.

• In the relatively small values of the ratio $E^{(1)}/E^{(2)}$ (in Case 4 Eq. (41) and Case 5 Eq. (42)) as a result of the non-axisymmetricity of the moving load, the dependence between the minimum critical velocity and h/R becomes non monotonic, however, in the relatively greater values of the ratio $E^{(1)}/E^{(2)}$ this dependence is monotonic and an increase in the values of the ratio h/R causes an increase in the values of the critical velocity;

• In all the considered cases, a decrease in the values of the ratio $E^{(1)}/E^{(2)}$ causes a decrease in the dimensionless critical velocity $V_{cr}/c_2^{(2)}$, where V_{cr} is the critical velocity of the moving load and $c_2^{(2)}$ is the shear wave propagation velocity in the cylinder material;

• The critical velocities related to the corresponding axisymmetric moving load and to the non- axisymmetric moving load approach each other and the critical velocity regarding the corresponding plane-strain state with decreasing of the ratio h/R;

• Absolute values of the interface stresses caused by the non-axisymmetric moving load increase monotonically with the velocity of this load;

• The absolute values of the interface stress decrease monotonically with increasing of the central angle α (Fig. 1(b)) within which the moving forces with constant vertical and zero horizontal components are distributed uniformly;

• The critical velocities do not depend on the aforementioned central angle;

• Among the interface stresses in the quantitative sense, the dominant role belongs to the normal stress;

• The absolute values of the interface stresses increase with decreasing of the ratio h/R;

• The character of the distribution of the normal interface stress in the circumferential direction depends on the value of the central angle, for instance, in the cases where $\alpha=\pi/36$ and $\pi/12$ the absolute maximum of the stress appears at $\theta=0$, however, in the case where $\pi/6$ and $\alpha=\pi/4$ this maximum appears at $\theta=\theta^*>0$;

• The values of $\theta=\theta^*$ at which the circumferential interface shear stress $\sigma_{r\theta}$ has its absolute maximum increase with the angle α;

• The decaying and the changing of the interface stresses with respect to the dimensionless moving coordinate z/h can also be taken as the decaying and the changing of these stresses with respect to time at a corresponding fixed interface point in the reference coordinate system;

• An increase in the values of the modulus of elasticity of the cylinder material under a fixed value for the surrounding elastic medium or a decrease in the values of the surrounding elastic medium under a constant value for the cylinder material causes a decrease in the values of the interface stresses.

References

Abdulkadirov, S.A. (1981), "Low-frequency resonance waves in a cylindrical layer surrounded by an elastic medium", *J. Min. Sci.*, **16**(3), 229-234.

Achenbach, J.D., Keshava, S.P. and Hermann, G. (1967), "Moving load on a plate resting on an elastic half-space", *Trans. ASME. Ser. E. J. Appl. Mech.*, **34**(4), 183-189.

Akbarov, S.D. and Ismailov, M.I. (2016a), "Dynamics of the oscillating moving load acting on the hydro-elastic system consisting of the elastic plate, compressible viscous fluid and rigid wall", *Struct. Eng. Mech.*, **59**(3), 403-430.

Akbarov, S.D. and Ismailov, M.I. (2016b), "Frequency response of a pre-stressed metal elastic plate under compressible viscous fluid loading", *Appl. Comput. Math.*, **15**(2), 172-188.

Akbarov, S.D. (2015), *Dynamics of Pre-Strained Bi-Material Elastic Systems: Linearized Three-Dimensional Approach*, Springer, Heidelberg, New York, U.S.A.

Akbarov, S.D., Guler, C. and Dincsoy, E. (2007), "The critical speed of a moving load on a pre-stressed load plate resting on a pre-stressed half-plan", *Mech. Compos. Mater.*, **43**(2), 173-182.

Akbarov, S.D. and Ilhan, N. (2008), "Dynamics of a system comprising a pre-stressed orthotropic layer and pre-stressed orthotropic half-plane under the action of a moving load", *Int. J. Sol. Str.*, **45**(14-15), 4222-4235.

Akbarov, S.D. and Ilhan, N. (2009), "Dynamics of a system comprising an orthotropic layer and orthotropic half-plane under the action of an oscillating moving load", *Int. J. Sol. Str.*, **46**(21), 3873-3881.

Akbarov, S.D., Ilhan, N. and Temugan, A. (2015), "3D Dynamics of a system comprising a pre-stressed covering layer and a pre-stressed half-space under the action of an oscillating moving point-located load", *Appl. Math. Model.*, **39**, 1-18.

Akbarov, S.D. and Ismailov, M.I. (2014), "Forced vibration of a system consisting of a pre-strained highly elastic plate under compressible viscous fluid loading", *CMES*: *Comput. Model. Eng. Sci.*, **97**(4), 359-390.

Akbarov, S.D. and Ismailov, M.I. (2015), "Dynamics of the moving load acting on the hydro-elastic system consisting of the elastic plate, compressible viscous fluid and rigid wall", *CMC*: *Comput. Mater. Contin.*, **45**(2), 75-105.

Akbarov, S.D. and Ismailov, M.I. (2017), "The forced vibration of the system consisting of an elastic plate, compressible viscous fluid and rigid wall", *J. Vibr. Contr.*, **23**(11), 1809-1827.

Akbarov, S.D. and Mehdiyev, M.A. (2017), "Forced vibration of the elastic system consisting of the hollow cylinder and surrounding elastic medium under perfect and imperfect contact", *Struct. Eng. Mech.*, **62**(1), 113-123.

Akbarov, S.D. and Mehdiyev, M.A. (2018a), "Influence of initial stresses on the critical velocity of the moving load acting in the interior of the hollow cylinder surrounded by an infinite elastic medium", *Struct. Eng. Mech.*, **66**(1), 45-59.

Akbarov, S.D. and Mehdiyev, M.A. (2018b), "The interface Stress field in the elastic system consisting of the hollow cylinder and surrounding elastic medium under 3D non-axisymmetric forced vibration", *CMC*: *Comput. Mater. Contin.*, **54**(1), 61-68.

Akbarov, S.D. and Panakhli, P.G. (2015), "On the discrete-analytical solution method of the problems related to the dynamics of hydro-elastic systems consisting of a pre-strained moving elastic plate, compressible viscous fluid and rigid wall", *CMES*: *Comput. Model. Eng. Sci.*, **108**(4), 89-112.

Akbarov, S.D. and Panakhli, P.G. (2017), "On the particularities of the forced vibration of the hydroelastic system consisting of a moving elastic plate, compressible viscous fluid and rigid wall", *Coupled Syst. Mech.*, **6**(3), 287-316.

Akbarov, S.D. and Salmanova, K.A. (2009), "On the dynamics of a finite pre-strained bi-layered slab resting on a rigid foundation under the action of an oscillating moving load", *J. Sound Vibr.*, **327**(3-5), 454-472.

Atluri, S.N. and Shen, S.P. (2002), *The Meshless Local Petrov-Galerkin (MLPG) Method*, Tech. Science Press.

Babich, S.Y., Glukhov, Y.P. and Guz, A.N. (1986), "Dynamics of a layered compressible pre-stressed half-space under the influence of moving load", *Int. Appl. Mech.*, **22**(9), 808-815.

Babich, S.Y., Glukhov, Y.P. and Guz, A.N. (1988), "To the solution of the problem of the action of a live load on a two-layer half-space with initial stress", *Int. Appl. Mech.*, **24**(8), 775-780.

Babich, S.Y., Glukhov, Y.P. and Guz, A.N. (2008a), "Dynamics of a pre-stressed incompressible layered half-space under load", *Int. Appl. Mech.*, **44**(3), 268-285.

Babich, S.Y., Glukhov, Y.P. and Guz, A.N. (2008b), "A dynamic for a pre-stressed compressible layered half-space under moving load", *Int. Appl. Mech.*, **44**(4), 388-405.

Chonan, S. (1981), "Dynamic response of a cylindrical shell imperfectly bonded to a surrounding continuum of infinite extent", *J. Sound Vibr.*, **78**(2), 257-267.

Dieterman, H.A. and Metrikine, A.V. (1997), "Critical velocities of a harmonic load moving uniformly along an elastic layer", *Trans. ASME. J. Appl. Mech.*, **64**(3), 596-600.

Dincsoy, E., Guler, C. and Akbarov, S.D. (2009), "Dynamical response of a prestrained system comprising a substrate and bond and covering layers to moving load", *Mech. Compos. Mater.*, **45**(5), 527-536.

Forrest, J.A. and Hunt, H.E.M. (2006), "A three-dimensional tunnel model for calculation of train-induced ground vibration", *J. Sound Vibr.*, **294**(4-5), 678-705.

Guz, A.N. (1999), *Fundamentals of The Three-Dimensional Theory of Stability of Deformable Bodies*, Springer, Berlin, Germany.

Hasheminejad, S.M. and Komeili, M. (2009), "Effect of imperfect bonding on axisymmetric elastodynamic response of a lined circular tunnel in poroelastic soil due to a moving ring load", *Int. J. Sol. Str.*, **46**(2), 398-411.

Hung, H.H., Chen, G.H. and Yang, Y.B. (2013), "Effect of railway roughness on soil vibrations due to moving trains by 2.5D finite/infinite element approach", *Eng. Struct.*, **57**, 254-266.

Hussein, M.F.M., François, S., Schevenels, M., Hunt, H.E.M., Talbot, J.P. and Degrande, G. (2014), "The fictitious force method for efficient calculation of vibration from a tunnel embedded in a multi-layered half-space", *J. Sound Vibr.*, **333**(25), 6996-7018.

Jensen, F.B., Kuperman, W.A., Porter, M.B. and Schmidt, H. (2011), *Computational Ocean Acoustic*, 2nd Edition, Springer, Berlin, Germany.

Kiani, K., Avili, H.G. and Kojorian, A.N. (2015), "On the role of shear deformation in dynamic behavior of a fully saturated poroelastic beam traversed by a moving load", *Int. J. Mech. Sci.*, **94**, 84-85.

Metrikine, A.V. and Vrouwenvelder, A.C.W.M. (2000), "Surface ground vibration due to a moving load in a tunnel: Two-dimensional model", *J. Sound Vibr.*, **234**(1), 43-66.

Ozisik, M., Mehdiyev, M.A. and Akbarov, S.D. (2018), "The influence of the imperfectness of contact conditions on the critical velocity of the moving load acting in the interior of the cylinder surrounded with elastic medium", *CMC*: *Comput. Mater. Contin.*, **54**(2), 103-136.

Parnes, R. (1969), "Response of an infinite elastic medium to traveling loads in a cylindrical bore", *J. Appl. Mech. Trans.*, **36**(1), 51-58.

Parnes, R. (1980), "Progressing torsional loads along a bore in an elastic medium", *Int. J. Sol. Struct.*, **36**(1), 653-670.

Pozhuev, V.I. (1980), "Reaction of a cylindrical shell in a transversely isotropic medium when acted upon by a moving load", *Sov. Appl. Mech.*, **16**(11), 958-964.

Quyang, H. (2011), "Moving load dynamic problems: A tutorial (with a brief overview)", *Mech. Syst. Sign. Pr.*, **25**(6), 2039-2060.

Sarvestan, V., Mirdamadi, H.D. and Ghayour, M. (2017), "Vibration analysis of cracked Timoshenko beam under moving load with constant velocity and acceleration by spectral finite element method", *Int. J. Mech. Sci.*, **122**, 318-330.

Sheng, X., Jones, C.J.C. and Thompson, D.J. (2006), "Prediction of ground vibration from trains using the wavenumber finite and boundary element methods", *J. Sound Vibr.*, **293**(3-5), 575-586.

Shi, L. and Selvadurai, A.P.S. (2016), "Dynamic response of an infinite beam supported by a saturated poroelastic half space and subjected to a concentrated load moving at a constant velocity", *Int. J. Sol. Str.*, **88**, 35-55.

Song, Q., Shi, J., Lui, Z. and Wan, Y. (2016), "Dynamic analysis of rectangular thin plates of arbitrary boundary conditions under moving loads", *Int. J. Mech. Sci.*, **117**, 16-29.

Sudheesh Kumar, C.P., Sujatha, C. and Shankar, K. (2015),

"Vibration of simply supported beams under a single moving load: A detailed study of cancellation phenomenon", *Int. J. Mech. Sci.*, **99**, 40-47.

Useche, J. and Alvarez, H. (2016), "Elastodynamic analysis of thick multilayer composite plates by the boundary element method", *CMES*: *Comput. Model. Eng. Sci.*, **107**(4), 287-316.

Yuan, Z., Bostrom, A. and Cai, Y. (2017), "Benchmark solution for vibration from a moving point source in a tunnel embedded in a half-space", *J. Sound Vibr.*, **387**, 177-193.

Zhenning, B.A., Liang, J., Lee, V.W. and Ji, H. (2016), "3D dynamic response of a multi-layered transversely isotropic half-space subjected to a moving point load along a horizontal straight line with constant speed", *Int. J. Sol. Str.*, **100**, 427-445.

Zhou, J.X., Deng, Z.C. and Hou, X.H. (2008), "Critical velocity of sandwich cylindrical shell under moving internal pressure", *Appl. Math. Mech.*, **29**(12), 1569-1578.

CC

Appendix A1

In this appendix, explicit expressions of the functions $b_{k1n}(r)$, $b_{k2n}(r)$, $b_{k3n}(r)$, $d_{k1n}(r)$, $d_{k2n}(r)$, $d_{k3n}(r)$, $c_{k1n}(r)$, $c_{k2n}(r)$ and $c_{k3n}(r)$, which enter into Eqs. (19) and (20) are given. These expressions are

$$b_{120}(r)=2(\frac{\lambda^{(1)}}{2\mu^{(1)}}(s(b_1^{(1)}-(\zeta_2^{(1)})^2a_1^{(1)})K_0(\zeta_2^{(1)}r)-$$

$$s(\zeta_2^{(1)})^2K_0^{"}(\zeta_2^{(1)}r)-s\frac{\zeta_2^{(1)}}{r}K_0^{'}(\zeta_2^{(1)}r)-s(\zeta_2^{(1)})^2K_0^{"}(\zeta_2^{(1)}r))$$

$$b_{130}(r)=2(\frac{\lambda^{(1)}}{2\mu^{(1)}}(s(b_1^{(1)}-(\zeta_3^{(1)})^2a_1^{(1)})K_0(\zeta_3^{(1)}r)-$$

$$s(\zeta_3^{(1)})^2K_0^{"}(\zeta_3^{(1)}r)-s\frac{\zeta_3^{(1)}}{r}K_0^{'}(\zeta_3^{(1)}r)-s(\zeta_3^{(1)})^2K_0^{"}(\zeta_3^{(1)}r))$$

$$b_{320}(r)=s^2\zeta_2^{(1)}K_0^{'}(\zeta_2^{(1)}r)+(b_1^{(1)}-a_1^{(1)}(\zeta_2^{(1)})^2)\zeta_2^{(1)}K_0^{'}(\zeta_2^{(1)}r)$$

$$b_{420}(r)=s^2\zeta_2^{(1)}K_0^{'}(\zeta_2^{(1)}r)$$

$$b_{330}(r)=s^2\zeta_3^{(1)}K_0^{'}(\zeta_3^{(1)}r)+(b_1^{(1)}-a_1^{(1)}(\zeta_3^{(1)})^2)\zeta_3^{(1)}K_0^{'}(\zeta_3^{(1)}r)$$

$$b_{430}(r)=s^2\zeta_3^{(1)}K_0^{'}(\zeta_3^{(1)}r)$$

$$b_{620}(r)=(b_1^{(1)}-(\zeta_2^{(1)})^2a_1^{(1)})K_0(\zeta_2^{(1)}r)$$

$$b_{630}(r)=(b_1^{(1)}-(\zeta_3^{(1)})^2a_1^{(1)})K_0(\zeta_3^{(1)}r)$$

$$b_{11n}(r)=2(\frac{n}{r}\zeta_1^{(1)}K_n^{'}(\zeta_1^{(1)}r)-\frac{n}{r^2}K_n(\zeta_1^{(1)}r)$$

$$b_{12n}(r)=2(\frac{\lambda^{(1)}}{2\mu^{(1)}}(s(b_1^{(1)}-(\zeta_2^{(1)})^2a_1^{(1)})K_n(\zeta_2^{(1)}r)$$

$$-s(\zeta_2^{(1)})^2K_n^{"}(\zeta_2^{(1)}r)+s\frac{n^2}{r^2}K_n(\zeta_2^{(1)}r)-$$

$$\frac{s}{r}\zeta_2^{(1)}K_n^{'}(\zeta_2^{(1)}r)-s(\zeta_2^{(1)})^2K_n^{"}(\zeta_2^{(1)}r))$$

$$b_{13n}(r)=2(\frac{\lambda^{(1)}}{2\mu^{(1)}}(s(b_1^{(1)}-(\zeta_3^{(1)})^2a_1^{(1)})K_n(\zeta_3^{(1)}r)$$

$$-s(\zeta_3^{(1)})^2K_n^{"}(\zeta_3^{(1)}r)+s\frac{n^2}{r^2}K_n(\zeta_3^{(1)}r)-$$

$$\frac{s}{r}\zeta_3^{(1)}K_n^{'}(\zeta_3^{(1)}r)-s(\zeta_3^{(1)})^2K_n^{"}(\zeta_3^{(1)}r))$$

$$b_{21n}(r)=-\frac{n^2}{r^2}K_n(\zeta_1^{(1)}r)-(\zeta_1^{(1)})^2K_n^{"}(\zeta_1^{(1)}r)+\frac{\zeta_1^{(1)}}{r}K_n^{'}(\zeta_1^{(1)}r)$$

$$b_{22n}(r)=s\frac{n}{r}\zeta_2^{(1)}K_n^{'}(\zeta_2^{(1)}r)-2s\frac{n}{r^2}K_n(\zeta_2^{(1)}r)+\zeta_2^{(1)}s\frac{n}{r}K_n^{'}(\zeta_2^{(1)}r)$$

$$b_{23n}(r)=s\frac{n}{r}\zeta_3^{(1)}K_n^{'}(\zeta_3^{(1)}r)-2s\frac{n}{r^2}K_n(\zeta_3^{(1)}r)+\zeta_3^{(1)}s\frac{n}{r}K_n^{'}(\zeta_3^{(1)}r)$$

$$b_{31n}(r)=-s\frac{n}{r}K_n(\zeta_1^{(1)}r)$$

$$b_{32n}(r)=s^2\zeta_2^{(1)}K_n'(\zeta_2^{(1)}r)+(b_1^{(1)}-(\zeta_2^{(1)})^2a_1^{(1)})K_n(\zeta_2^{(1)}r)$$

$$b_{33n}(r)=s^2\zeta_3^{(1)}K_n'(\zeta_3^{(1)}r)+(b_1^{(1)}-(\zeta_3^{(1)})^2a_1^{(1)})K_n(\zeta_3^{(1)}r)$$

$$b_{41n}(r)=\frac{n}{r}K_n(\zeta_1^{(1)}r)$$

$$b_{42n}(r)=-s\zeta_2^{(1)}K_n'(\zeta_2^{(1)}r)$$

$$b_{43n}(r)=-s\zeta_3^{(1)}K_n'(\zeta_3^{(1)}r)$$

$$b_{51n}(r)=-\zeta_1^{(1)}K_n'(\zeta_1^{(1)}r)$$

$$b_{52n}(r)=s\frac{n}{r}K_n(\zeta_2^{(1)}r)$$

$$b_{53n}(r)=s\frac{n}{r}K_n(\zeta_3^{(1)}r)$$

$$b_{61n}(r)=0$$

$$b_{62n}(r)=(b_1^{(1)}-(\zeta_2^{(1)})^2a_1^{(1)})K_n(\zeta_2^{(1)}r)$$

$$b_{63n}(r)=(b_1^{(1)}-(\zeta_3^{(1)})^2a_1^{(1)})K_n(\zeta_3^{(1)}r)$$

$$d_{120}(r)=2(\frac{\lambda^{(2)}}{2\mu^{(2)}}(s(b_1^{(2)}-(\zeta_2^{(2)})^2a_1^{(2)})I_0(\zeta_2^{(2)}r)$$

$$-s(\zeta_2^{(2)})^2I_0''(\zeta_2^{(2)}r)-s\frac{\zeta_2^{(2)}}{r}I_0'(\zeta_2^{(2)}r)-s(\zeta_2^{(2)})^2I_0''(\zeta_2^{(2)}r))$$

$$d_{130}(r)=2(\frac{\lambda^{(2)}}{2\mu^{(2)}}(s(b_1^{(2)}-(\zeta_3^{(2)})^2a_1^{(2)})I_0(\zeta_3^{(2)}r)$$

$$-s(\zeta_3^{(2)})^2I_0''(\zeta_3^{(2)}r)-s\frac{\zeta_3^{(2)}}{r}I_0'(\zeta_3^{(2)}r)-s(\zeta_3^{(2)})^2I_0''(\zeta_3^{(2)}r))$$

$$d_{320}(r)=s^2\zeta_2^{(2)}I_0'(\zeta_2^{(2)}r)+(b_1^{(2)}-a_1^{(2)}(\zeta_2^{(2)})^2)\zeta_2^{(1)}I_0'(\zeta_2^{(2)}r)$$

$$d_{420}(r)=s^2\zeta_2^{(2)}I_0'(\zeta_2^{(2)}r)$$

$$d_{330}(r)=s^2\zeta_3^{(2)}I_0'(\zeta_3^{(2)}r)+(b_1^{(2)}-a_1^{(2)}(\zeta_3^{(2)})^2)\zeta_3^{(2)}I_0'(\zeta_3^{(2)}r)$$

$$d_{430}(r)=s^2\zeta_3^{(2)}I_0'(\zeta_3^{(2)}r)$$

$$d_{620}(r)=(b_1^{(2)}-(\zeta_2^{(2)})^2a_1^{(2)})I_0(\zeta_2^{(2)}r)$$

$$d_{630}(r)=(b_1^{(2)}-(\zeta_3^{(2)})^2a_1^{(2)})I_0(\zeta_3^{(2)}r)$$

$$d_{11n}(r)=2(\frac{n}{r}\zeta_1^{(2)}I_n'(\zeta_1^{(2)}r)-\frac{n}{r^2}I_n(\zeta_1^{(2)}r)$$

$$d_{12n}(r)=2(\frac{\lambda^{(2)}}{2\mu^{(2)}}(s(b_1^{(2)}-(\zeta_2^{(2)})^2a_1^{(2)})I_n(\zeta_2^{(2)}r)-$$

$$s(\zeta_2^{(2)})^2I_n''(\zeta_2^{(2)}r)+s\frac{n^2}{r^2}I_n(\zeta_2^{(2)}r)-\frac{s}{r}\zeta_2^{(2)}I_n'(\zeta_2^{(2)}r)-s(\zeta_2^{(2)})^2I_n''(\zeta_2^{(2)}r))$$

$$d_{13n}(r)=2(\frac{\lambda^{(2)}}{2\mu^{(2)}}(s(b_1^{(2)}-(\zeta_3^{(2)})^2a_1^{(2)})I_n(\zeta_3^{(2)}r)-$$

$$s(\zeta_3^{(2)})^2I_n''(\zeta_3^{(2)}r)+s\frac{n^2}{r^2}I_n(\zeta_3^{(2)}r)-\frac{s}{r}\zeta_3^{(2)}I_n'(\zeta_3^{(2)}r)-s(\zeta_3^{(2)})^2I_n''(\zeta_3^{(2)}r))$$

$$d_{21n}(r)=-\frac{n^2}{r^2}I_n(\zeta_1^{(2)}r)-(\zeta_1^{(2)})^2I_n''(\zeta_1^{(2)}r)+\frac{\zeta_1^{(2)}}{r}I_n'(\zeta_1^{(2)}r)$$

$$d_{22n}(r)=s\frac{n}{r}\zeta_2^{(2)}I_n'(\zeta_2^{(2)}r)-2s\frac{n}{r^2}I_n(\zeta_2^{(2)}r)+\zeta_2^{(2)}s\frac{n}{r}I_n'(\zeta_2^{(2)}r)$$

$$d_{23n}(r)=s\frac{n}{r}\zeta_3^{(2)}I_n'(\zeta_3^{(2)}r)-2s\frac{n}{r^2}I_n(\zeta_3^{(2)}r)+\zeta_3^{(2)}s\frac{n}{r}I_n'(\zeta_3^{(2)}r)$$

$$d_{31n}(r)=-s\frac{n}{r}I_n(\zeta_1^{(2)}r)$$

$$d_{32n}(r)=s^2\zeta_2^{(2)}I_n'(\zeta_2^{(2)}r)+(b_1^{(2)}-(\zeta_2^{(2)})^2a_1^{(2)})I_n(\zeta_2^{(2)}r)$$

$$d_{33n}(r)=s^2\zeta_3^{(2)}I_n'(\zeta_3^{(2)}r)+(b_1^{(2)}-(\zeta_3^{(2)})^2a_1^{(2)})I_n(\zeta_3^{(2)}r)$$

$$d_{41n}(r)=\frac{n}{r}I_n(\zeta_1^{(2)}r)$$

$$d_{42n}(r)=-s\zeta_2^{(2)}I_n'(\zeta_2^{(2)}r)$$

$$d_{43n}(r)=-s\zeta_3^{(2)}I_n'(\zeta_3^{(2)}r)$$

$$d_{51n}(r)=-\zeta_1^{(2)}I_n'(\zeta_1^{(2)}r)$$

$$d_{52n}(r)=s\frac{n}{r}I_n(\zeta_2^{(2)}r)$$

$$d_{53n}(r)=s\frac{n}{r}I_n(\zeta_3^{(2)}r)$$

$$d_{61n}(r)=0$$

$$d_{62n}(r)=(b_1^{(2)}-(\zeta_2^{(2)})^2a_1^{(2)})I_n(\zeta_2^{(2)}r)$$

$$d_{63n}(r)=(b_1^{(2)}-(\zeta_3^{(2)})^2a_1^{(2)})I_n(\zeta_3^{(2)}r)$$

$$c_{120}(r)=2(\frac{\lambda^{(2)}}{2\mu^{(2)}}(s(b_1^{(2)}-(\zeta_2^{(2)})^2a_1^{(2)})K_0(\zeta_2^{(2)}r)-$$

$$s(\zeta_2^{(2)})^2K_0''(\zeta_2^{(2)}r)-s\frac{\zeta_2^{(2)}}{r}K_0'(\zeta_2^{(2)}r)-s(\zeta_2^{(2)})^2K_0''(\zeta_2^{(2)}r))$$

$$c_{130}(r)=2(\frac{\lambda^{(2)}}{2\mu^{(2)}}(s(b_1^{(2)}-(\zeta_3^{(2)})^2a_1^{(2)})K_0(\zeta_3^{(2)}r)-$$

$$s(\zeta_3^{(2)})^2K_0''(\zeta_3^{(2)}r)-s\frac{\zeta_3^{(2)}}{r}K_0'(\zeta_3^{(2)}r)-s(\zeta_3^{(2)})^2K_0''(\zeta_3^{(2)}r))$$

$$c_{320}(r)=s^2\zeta_2^{(2)}K_0'(\zeta_2^{(2)}r)+(b_1^{(2)}-a_1^{(2)}(\zeta_2^{(2)})^2)\zeta_2^{(1)}K_0'(\zeta_2^{(2)}r)$$

$$c_{420}(r)=s^2\zeta_2^{(2)}K_0'(\zeta_2^{(2)}r)$$

$$c_{330}(r)=s^2\zeta_3^{(2)}K_0'(\zeta_3^{(2)}r)+(b_1^{(2)}-a_1^{(2)}(\zeta_3^{(2)})^2)\zeta_3^{(2)}K_0'(\zeta_3^{(2)}r)$$

$$c_{430}(r)=s^2\zeta_3^{(2)}K_0'(\zeta_3^{(2)}r)$$

$$c_{620}(r)=(b_1^{(2)}-(\zeta_2^{(2)})^2a_1^{(2)})K_0(\zeta_2^{(2)}r)$$

$$c_{630}(r)=(b_1^{(2)}-(\zeta_3^{(2)})^2a_1^{(2)})K_0(\zeta_3^{(2)}r)$$

$$c_{11n}(r)=2(\frac{n}{r}\zeta_1^{(2)}K_n'(\zeta_1^{(2)}r)-\frac{n}{r^2}K_n(\zeta_1^{(2)}r)$$

$$c_{12n}(r)=2(\frac{\lambda^{(2)}}{2\mu^{(2)}}(s(b_1^{(2)}-(\zeta_2^{(2)})^2a_1^{(2)})K_n(\zeta_2^{(2)}r)-$$

$$s(\zeta_2^{(2)})^2K_n^{"}(\zeta_2^{(2)}r)+s\frac{n^2}{r^2}K_n(\zeta_2^{(2)}r)-$$

$$\frac{s}{r}\zeta_2^{(2)}K_n^{'}(\zeta_2^{(2)}r)-s(\zeta_2^{(2)})^2K_n^{"}(\zeta_2^{(2)}r))$$

$$c_{13n}(r)=2(\frac{\lambda^{(2)}}{2\mu^{(2)}}(s(b_1^{(2)}-(\zeta_3^{(2)})^2a_1^{(2)})K_n(\zeta_3^{(2)}r)-$$

$$s(\zeta_3^{(2)})^2K_n^{"}(\zeta_3^{(2)}r)+s\frac{n^2}{r^2}K_n(\zeta_3^{(2)}r)-$$

$$\frac{s}{r}\zeta_3^{(2)}K_n^{'}(\zeta_3^{(2)}r)-s(\zeta_3^{(2)})^2K_n^{"}(\zeta_3^{(2)}r))$$

$$c_{21n}(r)=-\frac{n^2}{r^2}K_n(\zeta_1^{(2)}r)-(\zeta_1^{(2)})^2K_n^{"}(\zeta_1^{(2)}r)+\frac{\zeta_1^{(2)}}{r}K_n^{'}(\zeta_1^{(2)}r)$$

$$c_{22n}(r)=s\frac{n}{r}\zeta_2^{(2)}K_n^{'}(\zeta_2^{(2)}r)-2s\frac{n}{r^2}K_n(\zeta_2^{(2)}r)+\zeta_2^{(2)}s\frac{n}{r}K_n^{'}(\zeta_2^{(2)}r)$$

$$c_{23n}(r)=s\frac{n}{r}\zeta_3^{(2)}K_n^{'}(\zeta_3^{(2)}r)-2s\frac{n}{r^2}K_n(\zeta_3^{(2)}r)+\zeta_3^{(2)}s\frac{n}{r}K_n^{'}(\zeta_3^{(2)}r)$$

$$c_{31n}(r)=-s\frac{n}{r}K_n(\zeta_1^{(2)}r)$$

$$c_{32n}(r)=s^2\zeta_2^{(2)}K_n^{'}(\zeta_2^{(2)}r)+(b_1^{(2)}-(\zeta_2^{(2)})^2a_1^{(2)})K_n(\zeta_2^{(2)}r)$$

$$c_{33n}(r)=s^2\zeta_3^{(2)}K_n^{'}(\zeta_3^{(2)}r)+(b_1^{(2)}-(\zeta_3^{(2)})^2a_1^{(2)})K_n(\zeta_3^{(2)}r)$$

$$c_{41n}(r)=\frac{n}{r}K_n(\zeta_1^{(2)}r)$$

$$c_{42n}(r)=-s\zeta_2^{(2)}K_n^{'}(\zeta_2^{(2)}r)$$

$$c_{43n}(r)=-s\zeta_3^{(2)}K_n^{'}(\zeta_3^{(2)}r)$$

$$d_{51n}(r)=-\zeta_1^{(2)}K_n^{'}(\zeta_1^{(2)}r)$$

$$c_{52n}(r)=s\frac{n}{r}K_n(\zeta_2^{(2)}r)$$

$$c_{53n}(r)=s\frac{n}{r}K_n(\zeta_3^{(2)}r)$$

$$c_{61n}(r)=0$$

$$c_{62n}(r)=(b_1^{(2)}-(\zeta_2^{(2)})^2a_1^{(2)})K_n(\zeta_2^{(2)}r)$$

$$c_{63n}(r)=(b_1^{(2)}-(\zeta_3^{(2)})^2a_1^{(2)})K_n(\zeta_3^{(2)}r)$$

where

Appendix A2

$$I_n^{'}(x)=\frac{\mathrm{d}I_n(x)}{\mathrm{d}x},\quad I_n^{"}(x)=\frac{\mathrm{d}^2I_n(x)}{\mathrm{d}x^2},$$

$$K_n^{'}(x)=\frac{\mathrm{d}K_n(x)}{\mathrm{d}x},\quad K_n^{"}(x)=\frac{\mathrm{d}^2K_n(x)}{\mathrm{d}x^2},$$

$$a_1^{(1)}=\frac{2+\lambda^{(1)}/\mu^{(1)}}{1+\lambda^{(1)}/\mu^{(1)}},$$

$$b_1^{(1)}=\frac{-s^2}{1+\lambda^{(1)}/\mu^{(1)}}+\frac{\rho^{(1)}}{\rho^{(2)}}\frac{\mu^{(2)}s^2}{\mu^{(1)}}\left(\frac{V}{c_2^{(2)}}\right)^2\frac{1}{1+\lambda^{(1)}/\mu^{(1)}}$$

$$a_1^{(2)}=\frac{2+\lambda^{(2)}/\mu^{(2)}}{1+\lambda^{(2)}/\mu^{(2)}}$$

$$b_1^{(2)}=\frac{-s^2}{1+\lambda^{(2)}/\mu^{(2)}}+s^2\left(\frac{V}{c_2^{(2)}}\right)^2\frac{1}{1+\lambda^{(2)}/\mu^{(2)}}$$